SAND REPORT

SAND2002-4231
Unlimited Release
Printed January 2003

Making the Connection Between Microstructure and Mechanics

Elizabeth A. Holm , Corbett C. Battaile, H. Eliot Fang, Thomas E. Buchheit and Gerald W. Wellman

Prepared by
Sandia National Laboratories
Albuquerque, New Mexico 87185 and Livermore, California 94550

Sandia is a multiprogram laboratory operated by Sandia Corporation,
a Lockheed Martin Company, for the United States Department of Energy's
National Nuclear Security Administration under Contract DE-AC04-94-AL85000.

Issued by Sandia National Laboratories, operated for the United States Department of Energy by Sandia Corporation.

Available to DOE and DOE contractors from
U.S. Department of Energy
Office of Scientific and Technical Information
P.O. Box 62
Oak Ridge, TN 37831

Telephone: (865)576-8401
Facsimile: (865)576-5728
E-Mail: reports@adonis.osti.gov
Online ordering: http://www.doe.gov/bridge

Available to the public from
U.S. Department of Commerce
National Technical Information Service
5285 Port Royal Rd
Springfield, VA 22161

Telephone: (800)553-6847
Facsimile: (703)605-6900
E-Mail: orders@ntis.fedworld.gov
Online order: http://www.ntis.gov/help/ordermethods.asp?loc=7-4-0#online

SAND2002-4231
Unlimited Release
Printed January 2003

Making the Connection Between Microstructure and Mechanics

Elizabeth A. Holm , Corbett C. Battaile, and H. Eliot Fang
Materials and Process Modeling and Computation

Thomas E. Buchheit
Mechanical Reliability and Melting

Gerald W. Wellman
Thermal/Fluids Engineering

Sandia National Laboratories
P. O. Box 5800
Albuquerque, NM 87185-1411 USA

Abstract

The purpose of microstructural control is to optimize materials properties. To that end, we have developed sophisticated and successful computational models of both microstructural evolution and mechanical response. However, coupling these models to quantitatively predict the properties of a given microstructure poses a challenge. This problem arises because most continuum response models, such as finite element, finite volume, or material point methods, do not incorporate a real length scale. Thus, two self-similar polycrystals have identical mechanical properties regardless of grain size, in conflict with theory and observations. In this project, we took a tiered risk approach to incorporate microstructure and its resultant length scales in mechanical response simulations. Techniques considered include low-risk, low-benefit methods, as well as higher-payoff, higher-risk methods. Methods studied include a constitutive response model with a local length-scale parameter, a power-law hardening rate gradient near grain boundaries, a local Voce hardening law, and strain-gradient polycrystal plasticity. These techniques were validated on a variety of systems for which theoretical analyses and/or experimental data exist. The results may be used to generate improved constitutive models that

explicitly depend upon microstructure and to provide insight into microstructural deformation and failure processes. Furthermore, because mechanical state drives microstructural evolution, a strain-enhanced grain growth model was coupled with the mechanical response simulations. The coupled model predicts both properties as a function of microstructure and microstructural development as a function of processing conditions.

Contents

1. Introduction: Making the Connection Between Microstructure and Mechanics

A material's chemical composition and processing history determine its microstructure; in turn, microstructure mediates the properties that control materials performance. Over the last two decades, mesoscale materials models have coupled chemistry and processing to microstructural evolution, and continuum mechanics models have utilized materials properties to predict engineering performance and reliability. However, the critical link – between microstructure and mechanical properties – has yet to be made.

Historically, many relationships between microstructural parameters and mechanical response have been explored. In general, these response functions are formulated in terms of some mean microstructural parameter that is easy to quantify in a metallographic cross-section. For example, the Hall-Petch function relates yield strength to mean grain size in metals.

Recently, computational materials modeling and quantitative metallography have developed to the point where microstructure may be characterized in far more detail. Parameters such as maximum and minimum feature sizes, feature topology and connectivity, neighbor correlations, and full spatial distributions may be obtained in two and three dimensions. Computational mechanical engineering has evolved simultaneously to the point that both constitutive models and element-based solvers can operate on complex materials systems. The underlying physics of elastic deformation and plastic flow are incorporated in constitutive models that include crystallography, dislocation motion, and complex hardening. The challenge is to link these models to create a predictive response model that includes the effects of microstructural complexity.

One obvious solution is to input a microstructure into a polycrystal plasticity finite element model (PPFEM). Such simulations yield a wealth of intriguing and useful data. For example, correlations between individual grain size and local stress elucidate mechanisms for damage initiation; a model that incorporates only a mean grain size could not capture such relationships.

However, current implementations of PPFEM have a major drawback, common to continuum mechanics models. Macroscopic stress/strain curves generated by PPFEM for two polycrystalline microstructures that differ only in average grain size are indistinguishable, which disagrees with the Hall-Petch relationship and real-world experiments. The problem is that *current continuum mechanics models do not include an intrinsic length scale.* In such models, the only difference between a small grain and a large grain is the number of volume elements in the grain. Therefore, given two statistically self-similar microstructures, the coarse-grained material is equivalent to a mesh-refined fine-grained material, so fine- and coarse-grained materials must behave identically. This problem also affects other length-scale-dependent properties, such as shear banding, fracture, and inhomogeneous plastic deformation. Because making a direct connection between microstructure and mechanical properties is a critical challenge in computational materials modeling, solving this problem is our top priority.

A number of attempts have been made to incorporate a real length scale in continuum mechanics models and simulations. These efforts range from simple (brute force) to esoteric (strain gradient with couple stresses); however, all have approached this problem from a continuum mechanics perspective and have focused on localization phenomena in the continuum (i.e. shear banding).

Materials science issues, particularly the coupling between microstructure and response, have never been addressed. Moreover, all of the methods which have been developed are research codes; none have been analyzed, documented and validated sufficiently to become a standard tool.

In this project, we take a tiered risk approach to incorporate microstructure and its resultant length scales in mechanical response simulations. There are five steps to this approach: (1) Identify candidate techniques via literature search, networking, etc. (2) Prioritize methods based on risks and potential benefits. (3) Explore chosen methods by implementation and testing. (4) Develop the most promising models as research codes for extensive analysis, validation, and verification. (5) Deploy successful techniques in Sandia mechanics toolsets. Note that at each step, some techniques may be eliminated from further consideration.

An international workshop was held in April 1999 at Sandia with a goal of performing some of the initial identification and prioritization of methods for incorporating a length scale in polycrystal plasticity continuum models (PPCM); PPCM includes both PPFEM and the microstructural materials point method (MMPM). Using information from our panel of experts, we formulated the plan shown in Table I.

Table I. Prioritized candidate techniques

Technique	*Risk*	*Pros*	*Cons*	*Action*
Include length-scale parameter in PPFEM constitutive model	Low	Fast, easy, follows continuum mechanics paradigm	Not predictive – hardwires the desired result; cannot resolve localization phenomena	Rejected as too simplistic
Incorporate grain boundary phase in MMPM simulation	Low	Phase fraction gives length scale; qualitatively reproduces localization phenomena	Not quantitative – reproduces phenomenology without physics	Not pursued due to project staffing change
Include a hardening rate gradient near grain boundaries in PPFEM	Low	Fast; follows continuum mechanics paradigm; gradient width sets length scale	Stress redistribution homogenizes load bearing; does not reproduce experimental observations	Rejected as physically incorrect
Include a local Voce hardening model in PPFEM (see section 2)	Medium	Voce exponent gives length scale; reproduces dislocation pileup phenomenology	Model parameters are constitutive, not fundamental; requires fitting to experimental data	Selected as a useful method for parametric studies
Develop strain-gradient plasticity model for PPFEM (see section 3)	Medium	Burgers vector gives intrinsic length scale; direct connection between microstructural features and strain localization	Large number of physical variables have not been measured; computationally intensive	Selected as a useful method for physics-based studies
Implement subgrain breakup model in PPFEM	High	Surface-to-volume gives length scale; incorporates real physics for strain localization	Hard to measure physical quantities required as input; computationally intensive	Not pursued due to project time constraints

Table I also indicates the action taken for each method under this project. Preliminary tests showed that including a length-scale term in the mechanical response constitutive function for each PPFEM volume element was fast, easy to implement, and reproduced the desired response. In particular, when the flow equation for each element was modified to include a Hall-Petch dependence of yield stress on grain size, the polycrystal as a whole displayed a Hall-Petch dependence of flow strength on average grain size. However, because this result is essentially hardwired in the constitutive model, it is physically unsatisfying. In addition, subgrain localization effects, such as hardening near grain boundaries, cannot be resolved by this method, as each element within a grain deforms like every other. Therefore, this method was rejected from further consideration.

As an alternative to modifying the PPCM constitutive model, the simulation can be altered to include a grain boundary phase that deforms differently from the bulk. If grain boundary width is constant, the boundary phase fraction implies a grain size. Our preliminary simulations of this type show strain localization near boundaries and length scale dependence. However, there are no physics included in this technique, so results are purely qualitative. This method was not pursued further due to a project staffing change.

Since grain size effects in plastic flow are proposed to originate from dislocation pile up near grain boundaries, we next devised a model that contains a gradient in power-law hardening rate near grain boundaries. The two adjustable parameters are the exponent and width of the hardening rate power-law; the width sets the length scale dependence in the model. Elements are assigned a hardening rate that depends on their distance from the nearest grain boundary. While near-boundary elements initially harden more quickly than interior elements, this preferential hardening causes strain to be redistributed to the soft elements. By 0.1% strain, the stress distribution has homogenized across the system. No stress localization or Hall-Petch behavior is observed. Since these results are in clear contradiction with experiments, this method was rejected as physically incorrect.

Power-law hardening is characterized by continually increasing hardness with strain. However, in real materials, hardness saturates due to recovery effects. Therefore, our next step was to replace the power-law hardening expression by a saturating Voce-based hardening function. In this model, the hardness of an element is related to its distance from the grain boundary taken to some exponent. Initially, we used an exponent of –1/2, in agreement with the macroscopic Hall-Petch exponent; however, this did not reproduce the experimentally observed Hall-Petch or stress-strain behavior. Subsequently, we used an exponent of –1, reflecting the boundary surface to volume ratio in a polycrystal. After fitting the other constitutive parameters to experimental data taken at one grain size, this law reproduced experimental data at many different grain sizes, and gave a Hall-Petch exponent very near 0.5. This method is discussed in detail in section 2.

Due to the success of the Voce hardening model, it was selected for further development in the JAS3D finite element code. Periodic boundary conditions were implemented to allow bulk-like test samples. Mesh sensitivity was tested for and eliminated. When implemented for a 2D randomly textured microstructure using parameters developed for copper, this simulation showed several intriguing features. As expected, stress initially concentrates near grain boundaries. As strain increases, a clear network of load-bearing grains forms, and the distribution of the average stress per grain widens. While the macroscopic stress across each grain appears fairly uniform,

the microscopic stresses within a grain can vary quite dramatically. That is, stress exhibits structure on two length scales: the microstructure scale and the subgrain scale.

Using the preliminary results of the Voce model simulations, a strain-enhanced microstructural evolution model was developed using the Front-Tracking method. Grains are grown for several timesteps, and the evolved microstructure is passed back to the PPFEM simulation for re-equilibration. This model is discussed in section 4.

Finally, models that resolve microstructural processes within a continuum framework promise the highest degree of physical realism. For example, the subgrain breakup model, developed by M. Ortiz at CIT, models the flow behavior of dislocation cell microstructures commonly observed in metals. All geometrically necessary dislocations are placed in cell walls. As deformation proceeds, dislocations are added to the cell walls until interfacial energy favors a split to two lower misorientation cell walls. The simple, single crystal implementation of this scheme has successfully reproduced the observation that subgrain size decreases with deformation. Hall-Petch behavior (as a function of cell size) is also seen. The subgrain breakup model includes substantially more physics than other candidate models, but it is the least physically developed. While it shows great promise, time constraints prevented investigating it during this project.

The results of a successful model fulfill three critical needs in computational materials science: (1) The macro response predicted by the model can be used to generate constitutive models which explicitly depend upon microstructure in order to improve traditional continuum mechanical response models. This enables the direct linking of microstructure to materials properties to system performance. (2) The microscopic structures formed under load answer questions about deformation and failure processes as a function of microstructure. For example, does the microscopic stress distribution scale with grain size, or does the grain size effect overwhelm the structural effect? Are critical levels of local strain achieved before macro strain reaches failure level? Is deformation homogeneous or does the material flow along certain paths of connected grains? (3) The interdependence of microstructure and mechanics at the grain and subgrain level provides new opportunities in process design and control. For example, texture predictions can be compared to measurements to elucidate the mechanical state achieved during a complex process. Likewise, deformation conditions may be altered to achieve a particular final grain size.

2. Microstructural Length Scale via Grain Boundary Hardening Models

2.1. Polycrystal Plasticity Finite Element Model (PPFEM)

A microstructure-based model capable of accurately simulating the deformation response of a polycrystalline material must not be so cumbersome that when it is implemented into finite element code it cannot solve a large scale problem, e.g. 100's of grains and ~100,000 elements, in a reasonable time frame, e.g. within a few hours or days. Also, the model must be defined such that a unique set of material parameters can be determined and the model results be validated from a series of relatively straightforward material deformation experiments. A crystal plasticity formulation has been implemented into Sandia National Laboratories JAS3D finite element code [1] with the goal of meeting these criteria. The general formulation adequately captures aspects of subgrain deformation by modeling local material deformation via the well-known slip mechanism in a (poly)crystalline material. In an FCC metal, a rate-dependent phenomenology has been developed which partitions plastic deformation amongst the crystallographic $\langle 111 \rangle \{ 110 \}$ slip systems defined within a single crystal. [2] Literature examples abound with FCC crystal plasticity formulations incorporated into finite element code, allowing researchers to mesh assemblages of crystals which more closely approximate the microstructural deformation response of a polycrystalline material.

A finite element implementation of a polycrystal plasticity model has the great advantage of allowing the finite element method to enforce compatibility and equilibrium between and within grains. Local intra- and intergranular response of grains within a simulated polycrystal are driven by geometric constraints imposed by neighboring grains with different orientations. Lattice rotation and material strength within each element is tracked, thus a finite element polycrystal plasticity simulation composed of several hundred elements per grain provides access to a large amount of local simulated microstructural information, e.g. [3-5]. Examples of simulated results using the JAS3D implementation of the polycrystal plasticity model are illustrated in figure 2.1. These examples include 3-D and paved 2-D finite element meshes composed of 200 randomly oriented grains, each grain typically containing several hundred elements, designed to look like a realistic microstructure subjected to boundary conditions periodic on all faces and meant to simulate a tensile test. By correctly choosing the parameters in the work-hardening portion of the model, the simulated polycrystalline response fits the experimental tensile response of a copper polycrystal well, as shown in figure 2.1(a). Large von Mises stress variations, predicted within both the 2-D and 3-D models are generated by the variable constraints imposed by grain neighbors with different crystallographic orientations, as illustrated in figure 2.1(b). These local stress variations have never been experimentally validated.

This quasi-continuum based phenomenology does not track the motion or evolution of discrete microstructural features such as dislocations or subgrain boundaries, thus it inherently lacks a length scale. Recently, formulations that capture the effect of strain gradients have been incorporated into the crystal plasticity framework [6-9] to capture non-local influences, thus capturing size scale effects, on the deformation response of single crystals and polycrystals. These models are complex and currently perform poorly in large scale finite element simulations. In this report, the basis for a non-local model similar in certain aspects to the strain gradient models developed by these previous researchers is developed, but in a much simpler, heuristic form more amenable to large-scale simulation.

2.2. Kinematic Framework

A brief discussion of the model may begin with describing distortion of a continuum using the velocity gradient, which can be additively decomposed into symmetric and skew-symmetric parts:

$$\mathbf{L} = \boldsymbol{\Omega} + \mathbf{D} \tag{2.1}$$

where, $\mathbf{D}$ is the symmetric deformation rate tensor and $\boldsymbol{\Omega}$ is the skew-symmetric spin rate tensor. Distortion of single crystals has been described as a combination of plastic flow due to crystallographic slip and lattice distortion. Lattice distortion includes elastic distortion and rigid body rotation of the crystal lattice. Thus, for single crystals the deformation rate, $\mathbf{D}$, and spin rate, $\boldsymbol{\Omega}$, can be further decomposed into lattice and plastic parts as follows:

$$\mathbf{D} = \mathbf{D}_l + \mathbf{D}_p \tag{2.2a}$$

$$\boldsymbol{\Omega} = \boldsymbol{\Omega}_l + \boldsymbol{\Omega}_p \tag{2.2b}$$

where, $\mathbf{D}_l$ represents the lattice deformation rate, and $\mathbf{D}_p$ represents the plastic deformation rate due to crystallographic slip. $\boldsymbol{\Omega}_l$ represents the lattice spin rate and $\boldsymbol{\Omega}_p$ represents the plastic spin rate. The plastic deformation rate and spin rate depend on the slip rates, $\dot{\gamma}_s$, for the active slip systems,

$$\mathbf{D}_p = \sum_{s=1}^{12} \dot{\gamma}_s \mathbf{P}_s \tag{2.3}$$

$$\boldsymbol{\Omega}_p = \sum_{s=1}^{12} \dot{\gamma}_s \mathbf{W}_s \tag{2.4}$$

$\mathbf{P}_s$ and $\mathbf{W}_s$ are the symmetric and skew-symmetric parts of the dyad which is formed from the lattice vectors for each slip system, defined as:

$$\mathbf{P}_s = \frac{1}{2}(\mathbf{d}_s \otimes \mathbf{n}_s + \mathbf{n}_s \otimes \mathbf{d}_s) \tag{2.5}$$

$$\mathbf{W}_s = \frac{1}{2}(\mathbf{d}_s \otimes \mathbf{n}_s - \mathbf{n}_s \otimes \mathbf{d}_s) \tag{2.6}$$

where, $\mathbf{d}_s$ represents a unit vector oriented in the slip direction for slip system s and $\mathbf{n}_s$ represents a unit vector normal to the slip plane for slip system s.

This model uses a constitutive relation originally given by Asaro and Rice [10,11] based on the assumption that the elastic lattice properties are unaffected by slip:

$$\overset{\nabla}{\boldsymbol{\sigma}}_l + \boldsymbol{\sigma}\, \mathrm{tr}(\mathbf{D}_l) = \mathbf{E} : \mathbf{D}_l \tag{2.7}$$

where, $\boldsymbol{\sigma}$ is the Cauchy stress, $\mathrm{tr}(\mathbf{D}_l)$ represents the trace of $\mathbf{D}_l$, and $\mathbf{E}$ is the fourth order elasticity tensor. $\overset{\nabla}{\boldsymbol{\sigma}}_l^*$ is the co-rotational stress rate formed on axes which spin with the crystal lattice, defined as:

$$\overset{\nabla}{\boldsymbol{\sigma}}_l = \dot{\boldsymbol{\sigma}} - \boldsymbol{\Omega}_l \cdot \boldsymbol{\sigma} - \boldsymbol{\sigma} \cdot \boldsymbol{\Omega}_l \tag{2.8a}$$

Asaro and Rice also express the constitutive relation in terms of the co-rotational stress rate formed on axes which spin with a material element:

$$\overset{\nabla}{\boldsymbol{\sigma}} + \boldsymbol{\sigma}\,\mathrm{tr}(\mathbf{D}_l) = \mathbf{E} : (\mathbf{D} - \mathbf{P}'\dot{\gamma}) \tag{2.8b}$$

where

$$\mathbf{P}' = \mathbf{P} + \mathbf{E}^{-1} : (\mathbf{W} \cdot \boldsymbol{\sigma} - \boldsymbol{\sigma} \cdot \mathbf{W}) \tag{2.8c}$$

Lattice vectors which characterize the slip systems are affected by lattice distortion. A variety of assumptions can be made concerning the evolution of the crystal lattice vectors. In this version of the kinetic formulation, the crystal lattice vectors are assumed to remain orthogonal unit vectors that simply rotate at the lattice spin rate.

$$\dot{\mathbf{d}}_s = \boldsymbol{\Omega}_l \cdot \mathbf{d}_s \tag{2.9a}$$

$$\dot{\mathbf{n}}_s = \boldsymbol{\Omega}_l \cdot \mathbf{n}_s \tag{2.9b}$$

To complete the constitutive model, equations for the slip rates, $\dot{\gamma}_s$, are needed. For the current implementation, a slip rate with a power-law dependence on the resolved shear stress as originally suggested by [12] was used.

$$\frac{\dot{\gamma}_s}{\dot{\gamma}_0} = \frac{\tau_s}{\kappa_s}\left|\frac{\tau_s}{\kappa_s}\right|^{(1/m-1)} \tag{2.10}$$

where, $\dot{\gamma}_0$ is the reference slip rate, m is the rate sensitivity factor, τ_s is the resolved shear stress on slip system s, and κ_s is an internal state variable which accounts for the hardening on slip system s. The initial value of κ_s on each slip system corresponds to the critical resolved shear stress on that system, i.e. the stress necessary on slip system s to activate slip in the rate insensitive limit. In the rate dependent model, it is sometimes referred to as the reference shear stress. The resolved shear stress, τ_s, for slip system s generated by an applied Cauchy stress, $\boldsymbol{\sigma}$, can be obtained using Schmid's equation:

$$\tau_s = \mathbf{P}_s : \boldsymbol{\sigma} \tag{2.11}$$

2.3. Hardening Model

Material hardening is captured at the slip system level by evolving the κ_s term in equation (2.10). For this study, all slip systems harden at the same rate based on an integral form of the hardening saturation law originally proposed by Voce [13-15], given by

$$\sigma_s = \sigma_0 + (\sigma_{sat} - \sigma_0)\left(1 - \exp(-\frac{\theta}{\sigma_{sat} - \sigma_0}\varepsilon_{pl})\right) \qquad (2.12)$$

where, κ_0 is equivalent to σ_0, an offset or yield stress, κ_{sat} is equivalent to σ_{sat}, the saturation stress, and θ governs the rate of work hardening. The integral Voce law was chosen because it better captures the saturation hardening response of polycrystalline FCC metals at high strains and because it is more amenable to adjustment for the length scale modeling.

As stated, this model allows all slip systems to harden equally. Previously developed slip system hardening models that harden slip systems equally invariably evolve material hardening using total shear accumulated on all of the slip systems as an evolution parameter, i.e. the algebraic sum of shears $\sum_s \gamma$ [3, 8, 16], an assumption with substantial validity since the algebraic sum of shears has significance beyond a relative measure of accumulated strain through its relationship to the Taylor factor [17]. (The Taylor factor is a parameter originally defined to relate slip system strength to the overall strength of a polycrystal.) In this model, the Taylor factor is used to bridge between the curve fit response parameters given in figure 2.1 and the slip system hardening response used in a simulation. Hardening is evolved through equivalent plastic strain rather than the algebraic sum of shears because it is straightforward to relate equivalent plastic strain in a material element to plastic strain derived from experimental data.

By using parameters for σ_0, σ_{sat}, and θ determined from the fit in figure 2.1, and dividing the incremental work hardening response by the Taylor factor, a slip system hardening model is obtained directly from a stress-strain curve. Figure 2.1 illustrates an extremely favorable comparison between the simulated tensile hardening response of a randomly textured polycrystal composed of 200 grains using this slip system hardening model derived through this curve fit method.

2.4.Polycrystal Plasticity Simulation with No Length Scale

Element paving along smooth grain boundaries allows mesh refinement across a wide range of mesh densities, however, paving is not possible with quadrihedral 3-D meshing. Thus, 1 element thick paved meshes generated at different degrees of refinement within the same polycrystal microstructure are used for most of the comparisons in this report. Each simulation was subjected to periodic boundary conditions on all faces of these simulations. In all other aspects, the deformation boundary conditions were meant to replicate a tension test and therefore were the same as those used in the simulation illustrated in figure 2.1, results are given in figures 2.2 and 2.3. The total number of elements in the three simulations given in figure 2.2 are 8792 elements, "the coarse mesh", 33771 elements, "the medium mesh" and 118507 elements, "the fine mesh". Figure 2.2 clearly shows that predicted local von Mises stress distributions within grains is mesh insensitive across this wide range of mesh refinement.

To track deformation evolution of the microstructure, the model kinematic framework, which tracks crystal lattice rotation of each finite element within a simulation, is utilized. Prior to imparting deformation in a simulation, each element within a grain is initialized to the same crystal lattice orientation. As deformation initiates and progresses, the crystal lattice rotates within each finite element as determined by the lattice spin rate, $\mathbf{\Omega}_l$ [defined in equation (2.2b)]. This rotation can be defined by a lattice rotation matrix with three independent variables, or a

rotation about a normalized axis –often referred to as an axis-angle pair. Figure 2.2 includes plots of the evolved deformation as a function of the rotation angle, henceforth referred to as the lattice misorientation, extracted from the axis-angle pair description of the crystal lattice rotation after 10% tensile strain. Similar to the von Mises stress distributions, during deformation rotation gradients emerge within grains and are mesh insensitive across the investigated range of mesh densities. Accordingly, misorientation between adjacent elements within pre-defined grains after a prescribed amount of deformation is highly mesh sensitive, i.e. more elements per grain results in smaller misorientations between each element. The explanation for this mesh insensitivity is straightforward. The simulation framework does not define an element size, a grain size or an element size to grain size ratio, or more generally, the model does not define a microstructural length scale.

2.5. Incorporating a Length Scale to capture Grain Boundary Strengthening in Polycrystal Plasticity Simulations

Mechanical strengthening of a polycrystal by grain boundaries is a well-known phenomena and is generally defined by the Hall-Petch relationship [18]:

$$\sigma = \sigma_0 + kd^{-1/2} \tag{2.14}$$

where σ is the strength of the polycrystal, σ_0 is an offset stress affiliated with the strength of the material with no grain boundaries, k is a constant and d is the average grain diameter of the polycrystal. Results in the previous section demonstrated that refining the mesh changes the element size to grain size ratio, but in a simulation with no length scale, grain boundary strengthening and its effects on local stress and microstructure deformation evolution cannot be captured. Also, the basic kinematics of polycrystal plasticity models do not readily provide a method to capture grain boundary strengthening, a fundamental and well-established strengthening mechanism in polycrystalline materials, raising questions regarding the validity of the subgrain stress and deformation predictions of these models. The goal of this part of the study was to incorporate a length scale into the model framework and generate results on finite element meshes comparable to the "no length scale" simulations used to generate the results given in figures 2.1 and 2.2, thus addressing questions about the role of length scale in polycrystal plasticity modeling.

An example of Hall-Petch strengthening in an FCC metal is given in figure 2.4, a series of tensile test stress-strain curves taken from polycrystalline copper samples with different grain sizes. These curves show that the Hall-Petch effect offsets the yield stress due to grain boundary-dislocation interactions, but does not change the work hardening response of a copper polycrystal. Dislocation motion is regarded as the prime source of low homologous temperature plastic deformation accommodation, therefore dislocation-grain boundary interactions at micro-plastic strain levels serve to locally strengthen material near grain boundaries. [19] Thus, a plausible approach to including the effect of grain boundaries in a polycrystal plasticity simulation is to incorporate a phenomenology which preferentially strengthens material near grain boundaries at the onset of plastic deformation.

The experimental stress-strain data shows an offset yield stress and nearly identical work hardening behavior for a typical polycrystalline material with different average grain sizes. To capture this in the polycrystal plasticity simulation, material strength is initialized at higher values based on the distance of a material element from the nearest grain boundary. Within the

model implemented for this project, it is evolved by modifying the Voce formulation originally given in equation (2.12).

$$\sigma_s = \left(\sigma_0 + \frac{k}{d^n} \right) + \Delta\left(1 - \exp(-\frac{\theta}{\Delta}\varepsilon_{pl})\right) \qquad (2.15a)$$

$$\Delta = \sigma_{sat} - \sigma_0 \qquad (2.15b)$$

where, k and n are constants with meaning comparable to that in the Hall-Petch equation (2.14), d is distance from the nearest grain boundary, and all other variables defined as they were in the original model equation (2.12).

In a fashion similar to fitting the slip system work hardening response to a single stress-strain curve discussed in the previous section, equation (2.15) could be fit to a series of stress-strain curves obtained from a polycrystalline material with several different grain sizes. This was not done for the simulations in this report because a straightforward bridging between polycrystalline response and slip system response could not be performed using the Taylor factor. Through empirical fitting, the follow constants were used: θ=580, Δ=310, k=35, κ_0= 3 MPa and series of simulations were run with n=1/2 and n=1. The finite element mesh used in these simulations was the same as used for the "coarse grained" simulations used in figure 2.2. The resulting simulated polycrystalline tensile stress-strain response for the same grain sizes listed in figure 2.4 is given in figure 2.5. The figure shows that increasing the exponent n, increases the dependence of grain size on the yield strength of the polycrystal. As intended, the work hardening response of the simulated stress strain curves is not influenced by the grain size, following the same trend observed in the experimental data presented in figure 2.4.

The role of the exponent n in equation (2.15) on local slip system strength in the near grain boundary region of a polycrystal, is shown in figure 2.6. The boundary influence extends further into the grain as the value of n is increased. Clearly, increasing n increases the role of grain boundaries in the deformation response of the polycrystal and forces the increased dependence of grain size on the yield strength of the polycrystal. Figure 2.6 also illustrates a few weaknesses in the model, Each curve crosses at d =1 μm indicating an unwanted normalization in this model and vanishingly thin grain boundaries that have an infinite strength; thus grain boundaries represent singularities in the finite element simulations. By plotting yield strength vs. grain size for the experimental data, the simulated data with n=1/2 and the simulated data with n=1 (yield strength was measured using a 0.02 offset criterion on the simulated curves) the plot given in figure 2.7 was obtained. The slope of these curves gives the Hall-Petch exponent, accepted as 0.5 in the Hall-Petch relationship given in equation (2.14), for each series of polycrystals. Table I lists the measured Hall-Petch exponent obtained from the experimental data and both sets of simulations. The simulations which used n=1 gave a Hall-Petch exponent of 0.482, very close to the accepted value of 0.5 and to the measured value of 0.577 for the tensile stress-strain data measured from copper polycrystals.

Empirically, the polycrystal plasticity model with the added grain boundary length scale accurately replicated the stress-strain response of copper polycrystals with different average grain sizes when n=1. However, representing the grain boundaries as vanishingly thin discontinuities with infinite strengths creates a mesh sensitivity problem which cannot be overlooked.

Slip system strength distribution plots, illustrated in figure 2.8 show that as overall applied stress is increased differences in stress distribution between simulations with different grain sizes diminish. This observation corresponds with marching up the stress-strain curves, as the material work hardens the influence of grain boundary strengthening becomes a smaller percentage of the overall material strength. Similar behavior is seen in orientation space, as shown in figure 2.9.

2.6.A Mesh Independent Offset Model

To overcome mesh sensitivity caused by vanishingly thin and infinitely strong grain boundaries, an additional length scale was added to the model. The length scale gave grain boundaries a finite thickness and strength and amounted to a straightforward modification of equation (2.15):

$$\sigma_s = \left(\sigma_0 + \frac{k}{\max(\delta, d)^n} \right) + \Delta\left(1 - \exp(-\frac{\theta}{\Delta}\varepsilon_{pl})\right) \qquad (2.16)$$

where, δ is the new length scale which has the effect of capping the original grain boundary strengthening law, depicted in figure 2.10, such that the grain boundary has a finite strength. The value of δ corresponds to a grain boundary thickness. The indicator "max" takes the maximum value of δ or d, distance from the center of the nearest grain boundary. For the simulated results presented in this section, δ was set to 0.030 μm, which approximates grain sizes which Hall-Petch breakdown is observed in mechanical properties studies of nanocrystalline FCC metals [20-22]. All other parameters remained the same as used for the simulations in the previous section: κ_0=6.21 MPa, k=35, n=1, θ=580 and Δ=31. This new model is referred to as the "offset" model when compared to the "original" model presented in the previous section.

Figure 2.11(a) compares the simulated tensile stress-strain response of the 30 grain polycrystal with an average grain size of 15 μm using the original and offset grain boundary strengthening models. The offset model gives a slightly softer work hardening response, a consequence of capping the strength of the grain boundaries. Material very near or within the grain boundaries in the offset simulations is slightly softer than in the original simulations. Figure 2.11(b) illustrates that mesh independence can be achieved using the offset model. This figure shows a virtually indistinguishable tensile stress-strain response of a polycrystalline simulation with an average grain size of 1 μm using the "coarse", "medium" and "fine" meshes previously defined in figure 2.2. With mesh dependence eliminated, subsequent offset model simulations presented in this section use the "coarse" mesh.

Focusing on the importance of capturing Hall-Petch breakdown and nanocrystalline materials, the offset model was exercised at grain sizes between 0.01 - 1 μm. The simulated tensile stress-strain response of identical polycrystals spanning this grain size range is given in figure 2.12(a). The corresponding yield strength vs. grain size plot is given in figure 2.12(b). Both parts of figure 2.12 indicate a saturated strengthening response as the grain size approaches and drops below the value set for the δ parameter. Before saturation, the slope of the curve in the yield stress vs. grain size plot gives a Hall-Petch exponent, n = 0.735, slightly higher than the accepted value of 0.5 for polycrystalline FCC metals and also higher than the n = 0.482 value obtained from the original model results given in the previous section. The original model results were mesh sensitive suggesting that if this modified offset model offers a better

phenomenological approximation of true polycrystalline behavior, the constants κ_0, k, n in the local grain boundary strengthening model require a slight adjustment.

Figures 2.13 and 2.14 compare spatially resolved slip system strength and misorientation distribution in identical polycrystals with a 15 μm grain size using both original and offset models. The overall strength distribution is very similar between both models, but slightly higher in the original model, presumably because the grain boundaries have higher (infinite) strength in the original model. Figure 2.14 shows that the crystallographic misorientation distribution is very different when comparing both models. The offset model is a fairly minor modification of the original model, thus the significant difference in misorientation distribution between both models suggest that deformation evolution of microstructure is an unstable process. Also, evidence of deformation induced substructure not present in any of the previous results begins to appear within a few grains in the offset model. One example of deformation induced substructure showing bands of misorientation within a grain after 40% deformation is shown in figure 2.14.

Figures 2.15 through 2.17 illustrate the slip system strength distribution and spatially resolved misorientation of selected results based on grain size, ranging from 0.01 – 1 μm, using the offset model. Figure 2.15 illustrates that at grain sizes smaller than δ, i.e. 0.01 and 0.02 μm grain sizes, the spatial distribution of slip system strength does not vary and the spatial distribution of crystallographic misorientation is identical. At all locations in these simulations, material resides within a grain boundary because the grain size is less that the prescribe grain boundaries thickness, and slip system strength is initialized to the grain boundary value of 1173 MPa. These ultra-fine grained materials are initialized at near saturation as governed by equation (2.16) at all locations in the simulations, thus there is little opportunity for work hardening. The stress-strain curves given in figure 2.12 show the expected response for the small grain sizes, by illustrating a high yield strength and little work hardening before the onset of necking. There is no fracture criterion in the finite element model, thus the periodic boundary conditions imposed on the simulations enforce a stable diffuse neck.

Figures 2.16 and 2.17 show the spatially resolved slip system strength and crystallographic misorientation distribution in simulations with average grain sizes of 0.1 μm, 0.5 μm and 1 μm at strains of 0.1 and 0.4. Figure 2.16 illustrates that slip system strength varies widely across the different grain sizes and varies widely from the grain boundary to center of a grain. Obviously, the influence of a grain boundary extends further into a grain as the grain size is reduced. As opposed to the relatively uninformative result presented in figure 2.16, figure 2.17 illustrates several examples of deformation-induced substructure which resembles experimentally observed deformation bands and cell-blocks commonly observed in deformed polycrystals. Size scale plays a role in these results, as best illustrated by considering the largest grain in each of the three simulations. As the grain size increases the number of bands which form within a grain is increased as well. This observation of predicted substructure evolution is unique to this implementation of polycrystal plasticity modeling.

2.7.References for Section 2

1. Holm, E.A., Battaile, C.C., Buchheit, T.E., Fang, H.E. Rintoul, M.D., Vedula, V.R., Glass, S.J., Knorovsky, G.A., Neilsen, M.K. Wellman, G.W., Sulsky, D.L. "Computational Methods for Coupling Microstructural and Micromechanical Materials Response Simulations" SAND2000-1015, Sandia National Laboratories, Albuquerque, NM.

2. Kocks, U.F., Tome, C.N. and Wenk, H.R. "Texture and Anisotropy: Preferred Orientations in Polycrystals and Their Effect on Materials Properties", Cambridge University Press, 1998.

3. Mika, D.P. and Dawson, P.R., Materials Science and Engineering, vol. A257, 1998, p62-75.

4. Mika, D.P., and Dawson, P.R., Acta Mater., vol. 47, no. 4, 1999, pp. 1355-1369.

5. Barbe, F, Deeker, L., Jevlin D., Cailletaud, G., International Journal of Plasticity, vol. 17, 2001, p513-566.

6. Shu, J.Y., Fleck, N.A., Journal of the Mechanics and Physics of Solids, vol. 47, 1999, pp. 297-324.

7. Arsenlis A. and Parks, D.M., Journal of the Mechanics and Physics of Solids, vol. 50, 2002, pp.1979-2009.

8. Acharya, A., and Beaudoin, A.J., Journal of the Mechanics and Physics of Solids, vol. 48, 2002, pp. 2213-2230.

9. Bammann, D.J., Materials Science and Engineering A, vol. 309, 2001, pp. 406-410.

10. Asaro, R.J. and Rice, J.R., J. Mech. Phys. Solids, vol. 25, 1977, pp. 309-38.

11. Hill, R. and Rice, J.R., J. Mech. Phys. Solids, vol. 20, 1972, p401-420.

12. Hutchinson, J.W., Proc. R. Soc. A, vol 348, 1976, pp. 101-127.

13. Voce, E. "The Relationship Between Stress and Strains for Homogeneous Deformation", Journal of the Institute of Metals, vol. 74, 1948, pp. 537-562.

14. Voce, E. "A Practical Strain-Hardening Function", Metallurgica, vol. 51, 1955, pp. 219-226.

15. Kocks, U.F., Transactions of the ASME- Journal of Engineering Materials and Technology, 1976, pp 76-85.

16. Inal K., Wu P.D. and Neale, K.W., International Journal of Plasticity, vol. 16, 2000, pp. 635-648.

17. Mecking H., Kocks, U.F., Hartig, C.H., Scripta Materialia, Vol. 35, No. 4, 1996, pp. 465-471.

18. Dieter, G., "Mechanical Metallurgy", McGraw-Hill, 1986.

19. Li, J.C.M. and Chow, Y.T., Metallurgical Transactions, vol. 1, 1970, pg. 1145-1159.

20. Youngdahl, C.J., Weertmann, J.R., Hugo, R.C. and Kung, H.H., Scripta mater., vol. 44, 2001, pp. 1475-1481.

21. Wang, N. , Wang, Z., Aust, K.T., Erb, U., Acta metall. mater., vol. 43, no. 2, pp. 519-528, 1995.

22. Liu, X.D., Nagumo M., and Umemato, M., Materials Transactions JIM, vol. 38, no. 12, 1997, pp. 1033-1039.

2.8. Figures for Section 2

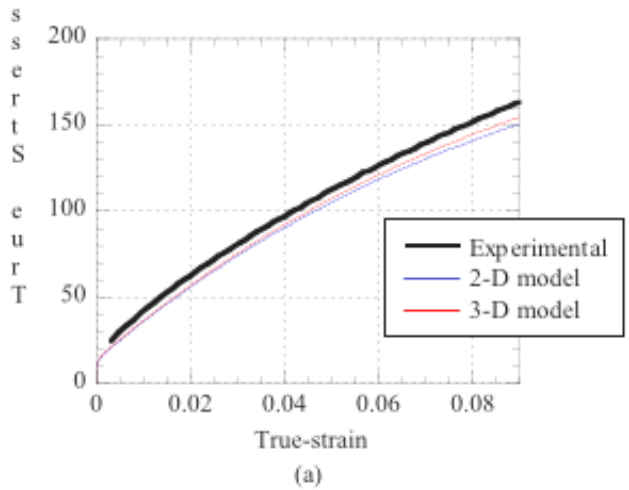

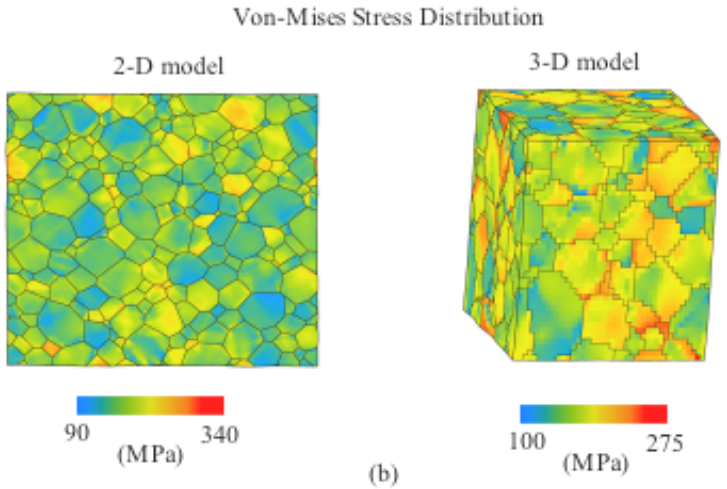

Figure 2.1 (a) Experimental and simulated tensile stress-strain response of a Copper polycrystal. Simulated response determined by 2-D and 3-D polycrystal plasticity models. (b) Predicted Von-Mises stress distribution in simulated polycrystals after 10% strain.

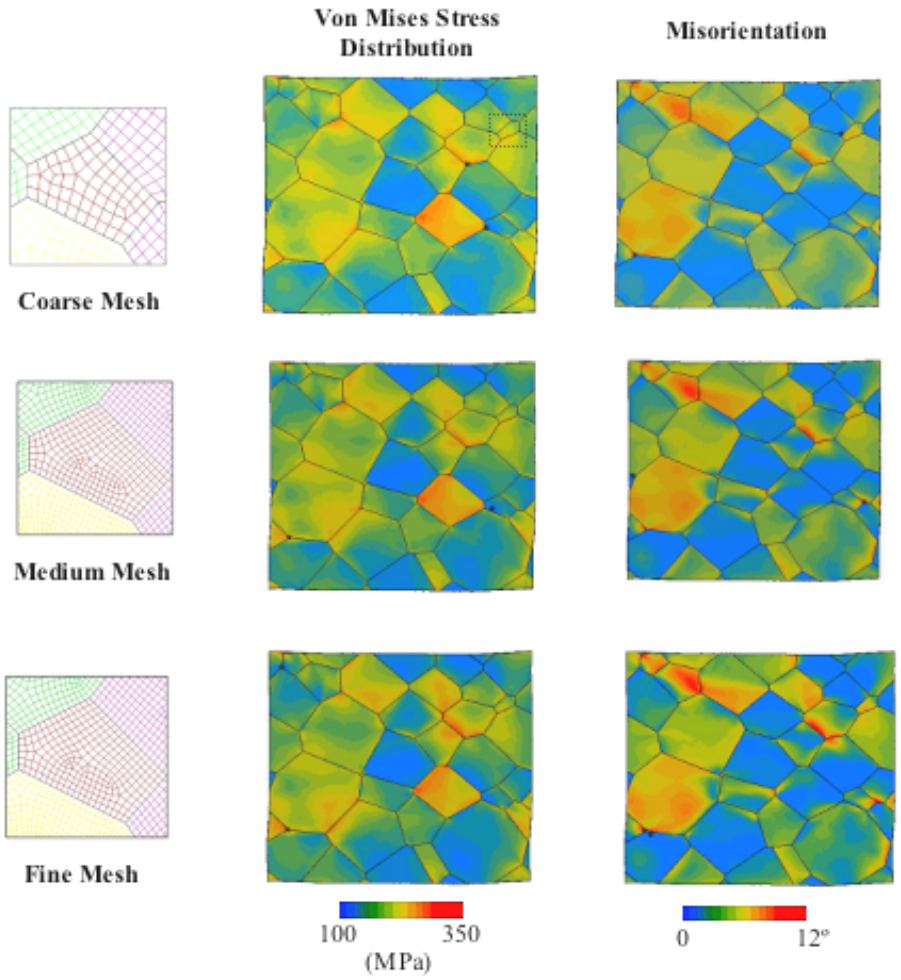

Figure 2. 2 – The effect of mesh refinement on stress distribution and local crystallographic misorientation in a polycrystal plasticity model.

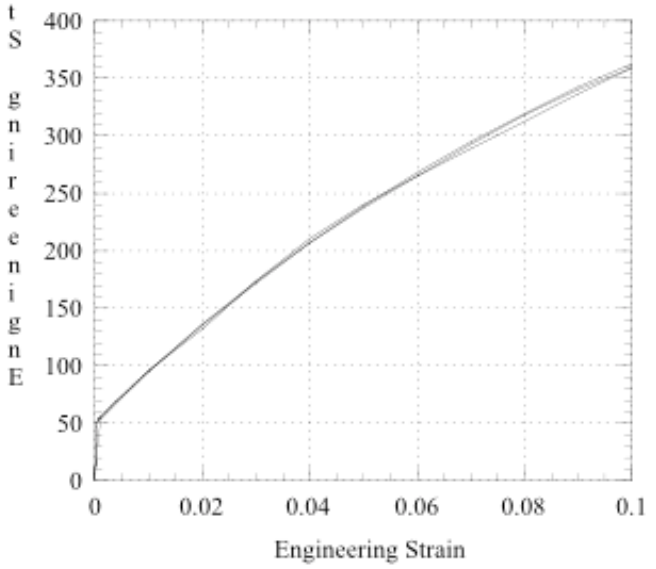

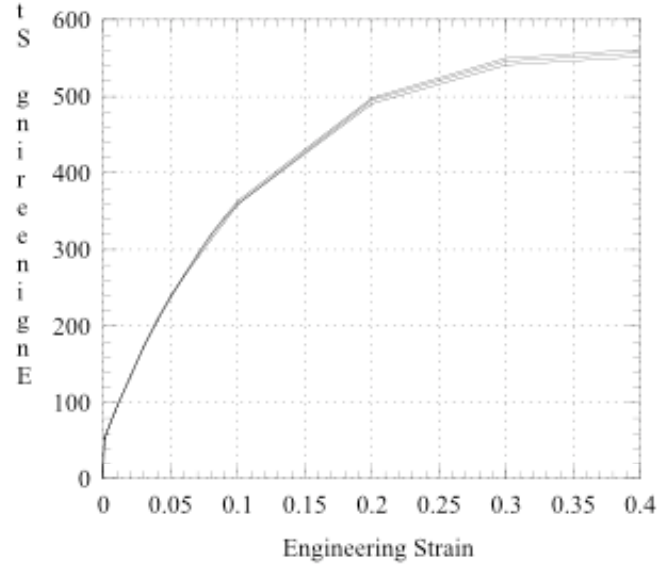

Figure 2. 3– Simulated stress-strain curves using polycrystal plasticity model on the same microstructure section with 3 different levels of mesh refinement given in figure 2.

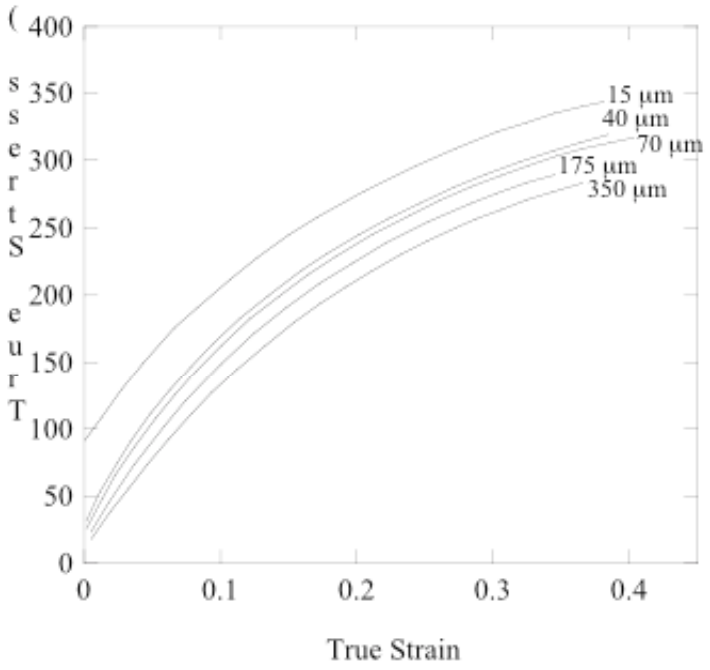

Figure 2. 4 - Hall-Petch strengthening in polycrystalline Copper, curves adapted from Fernandes and Viera. [00Vie]

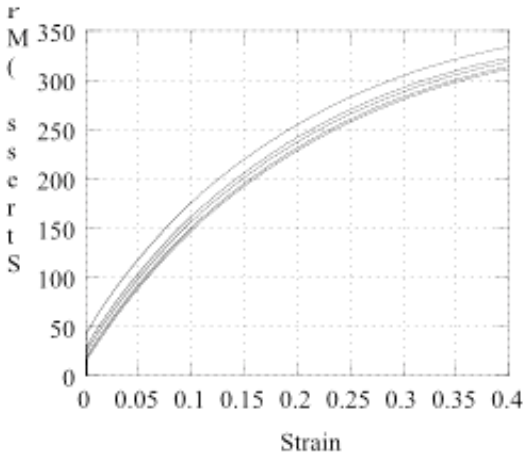

(a)

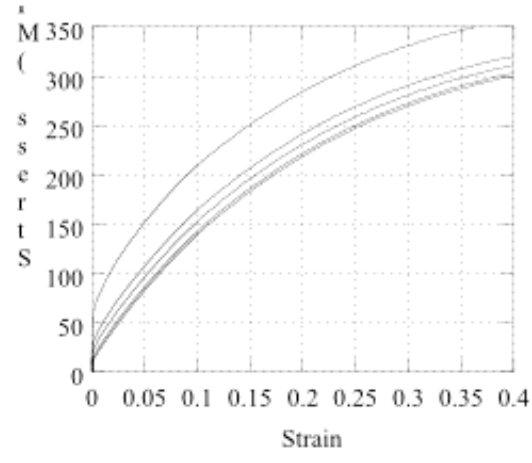

(b)

Figure 2. 5 - Simulated polycrystalline stress-strain response using grain size as a length scale in the work hardening portion of the polycrystal plasticity model, as expressed in equation 15. (a) results for n=1/2 and (b) results for n=1 in equation 15.

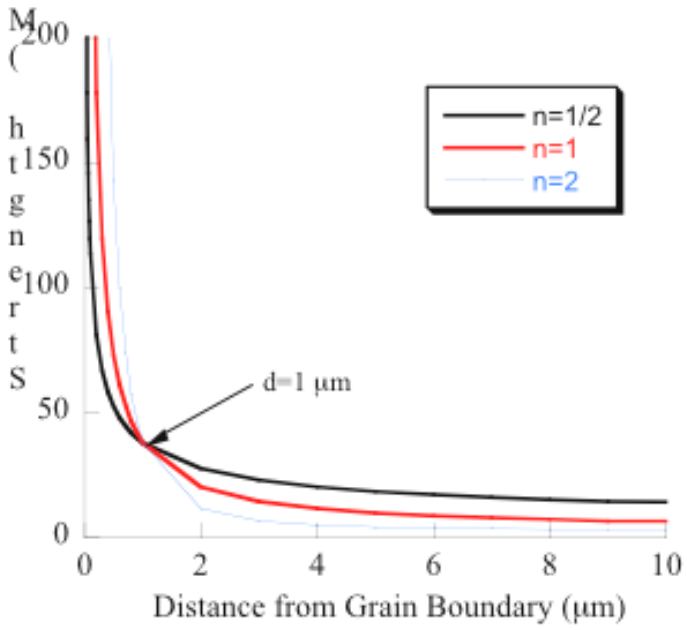

Figure 2. 6 - Local Grain Boundary Strengthening Law implemented into polycrystal plasticity model

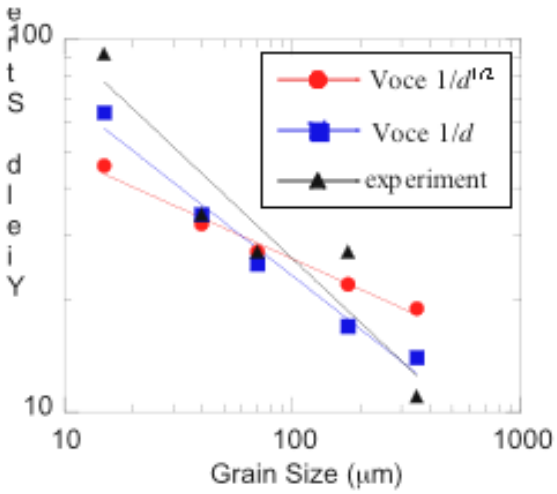

Figure 2. 7 – Yield Stress vs. Grain Size, experimental data and simulated results

Table I
Hall-Petch exponent obtained from simulated and experimental data

Model	Hall-Petch exponent
Voce $1/d^{1/2}$	-0.276
Voce $1/d$	-0.482
experiment	-0.577

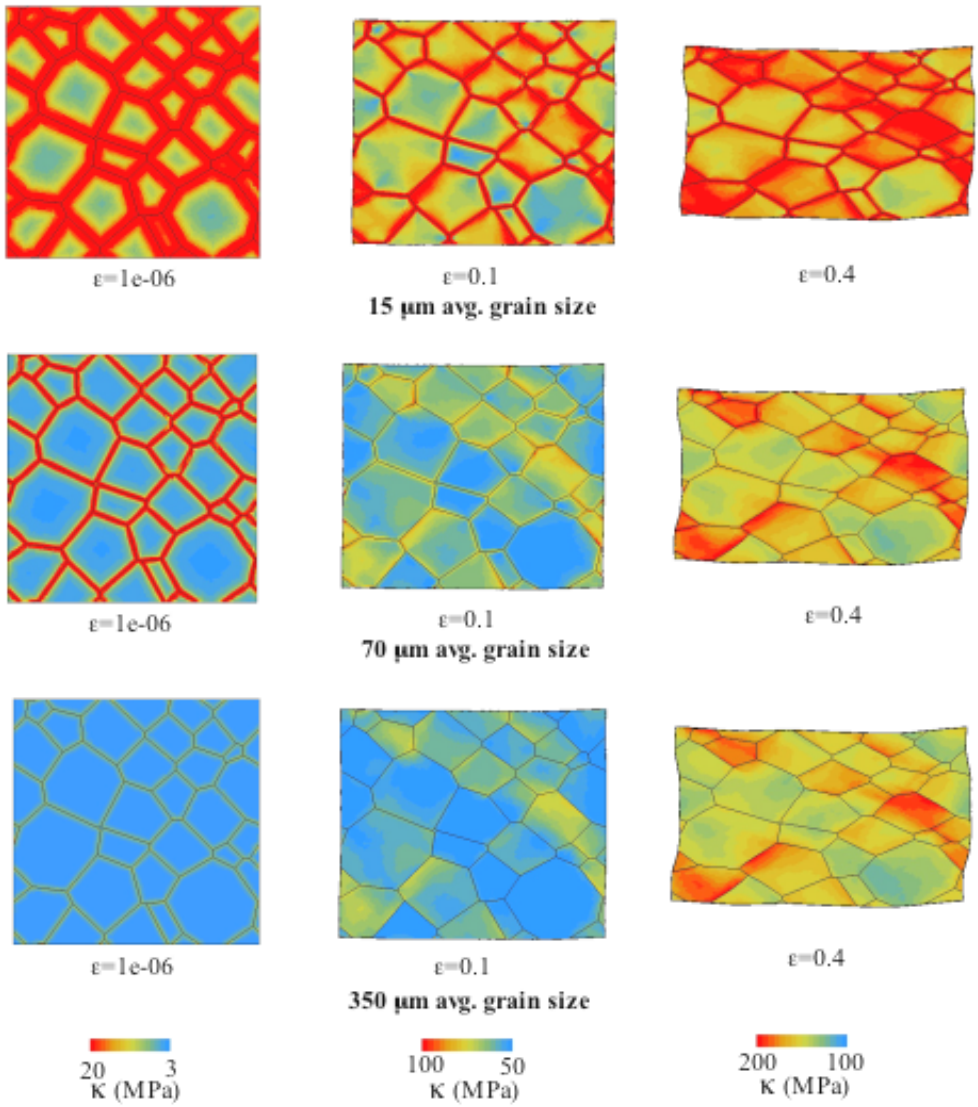

Figure 2. 8 - Slip system strength distribution at tensile strains of 1e-06, 0.1 and 0.4 for polycrystals with average grain sizes of 15 μm, 70 μm and 350 μm.

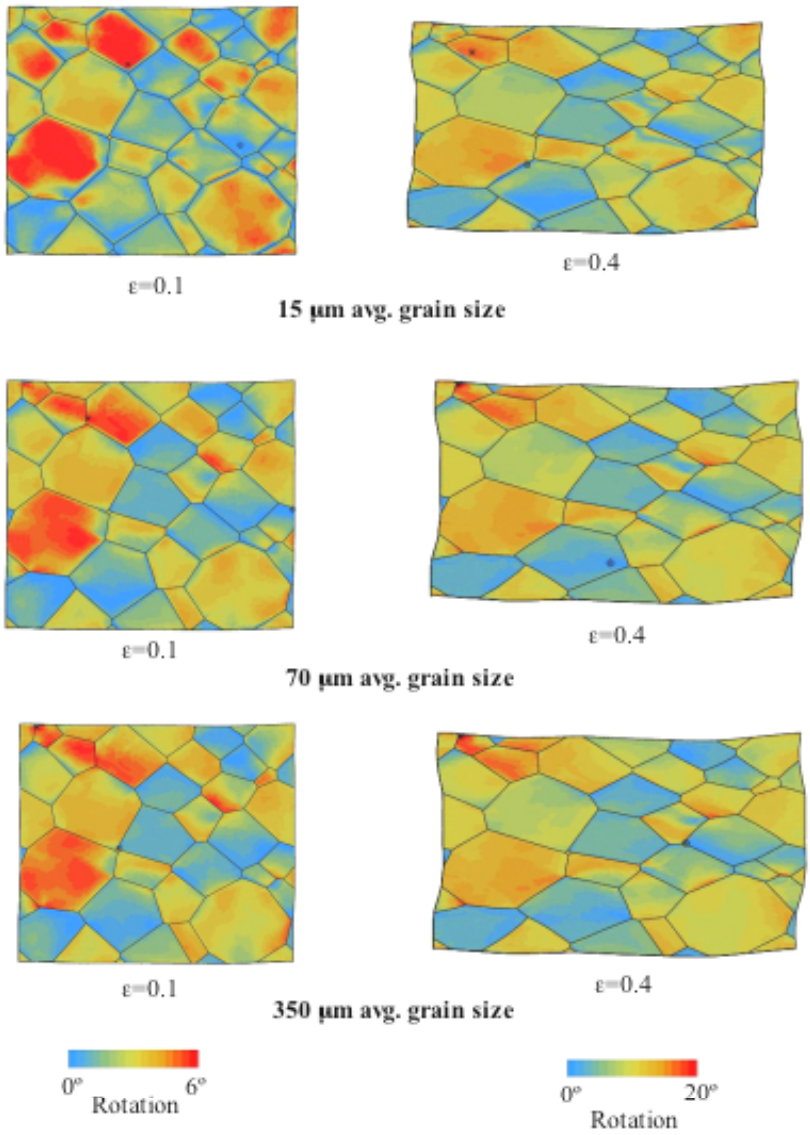

Figure 2. 9 - Spatially resolved crystallographic misorientation relative to original grain orientation at tensile strains 0.1 and 0.4 for polycrystals with average grain sizes of 15 μm, 70 μm and 350 μm.

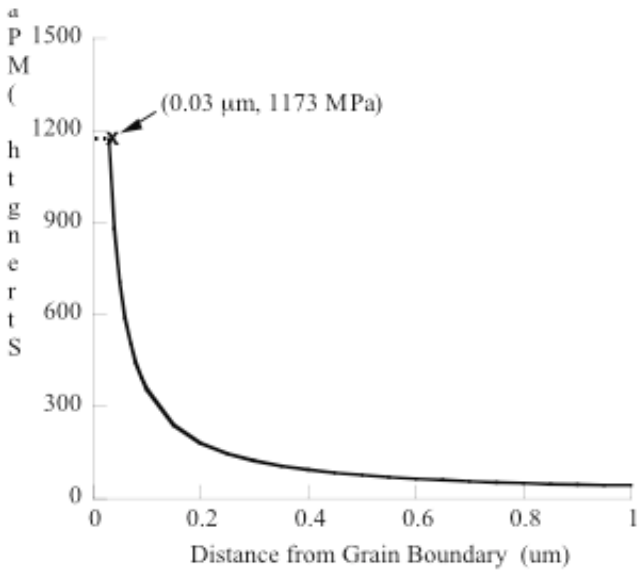

Figure 2. 10 - Modified "offset" local grain boundary model with the offset parameter, δ=0.03 μm. This model defines grain boundary thickness and grain boundary strength as additional parameters.

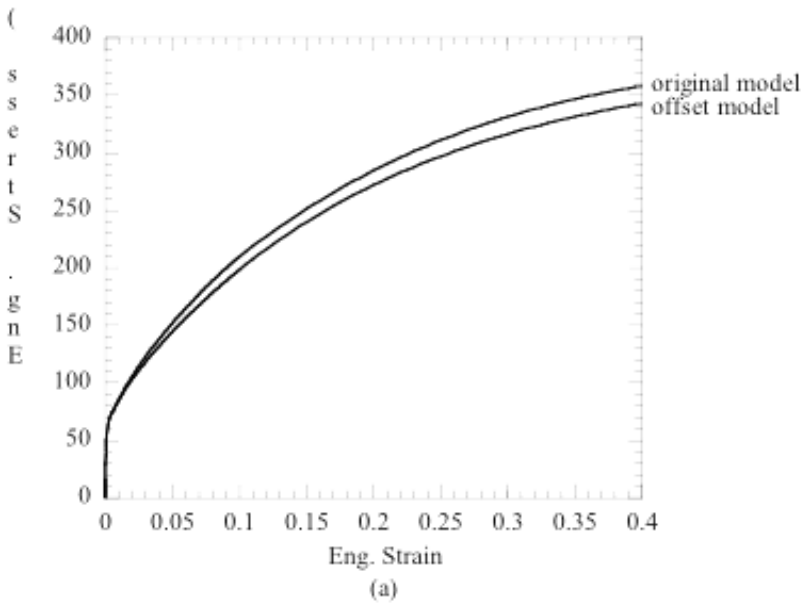

(a)

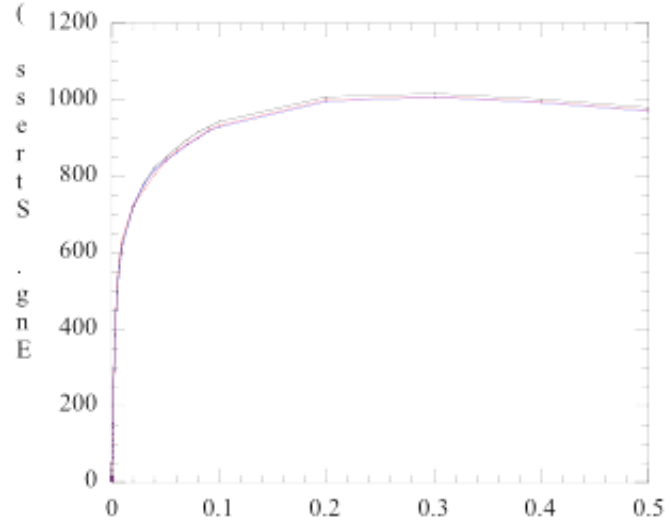

(b)

Figure 2. 11 (a) Comparison tensile stress-strain response in polycrystal simulations with an average grain size of 15 μm using the original and offset grain boundary strengthening models. (b) Comparison of tensile stress-strain response in polycrystal simulations with an average grain size of 1 μm using offset grain boundary strengthening model.

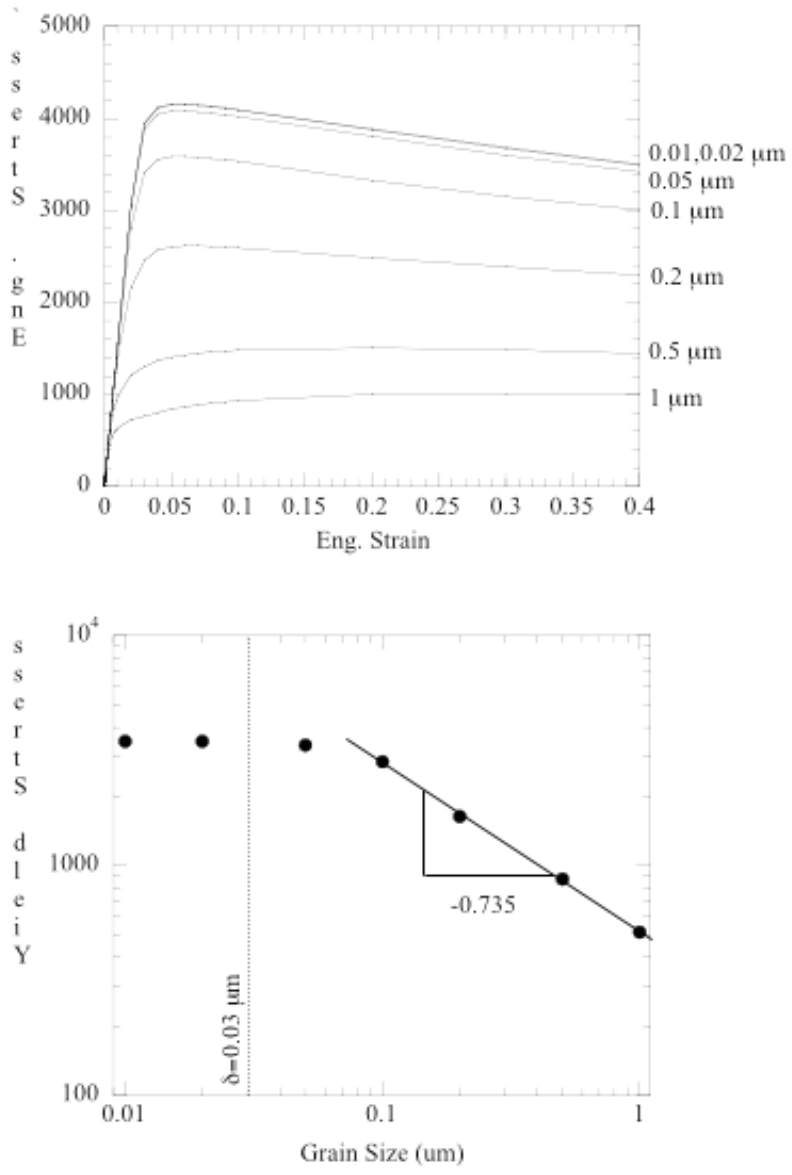

Figure 2. 12 - (a) Tensile stress-strain curves of simulated polycrystals with grain sizes between 0.01-1 μm. (b) corresponding yield strength vs. grain size plot.

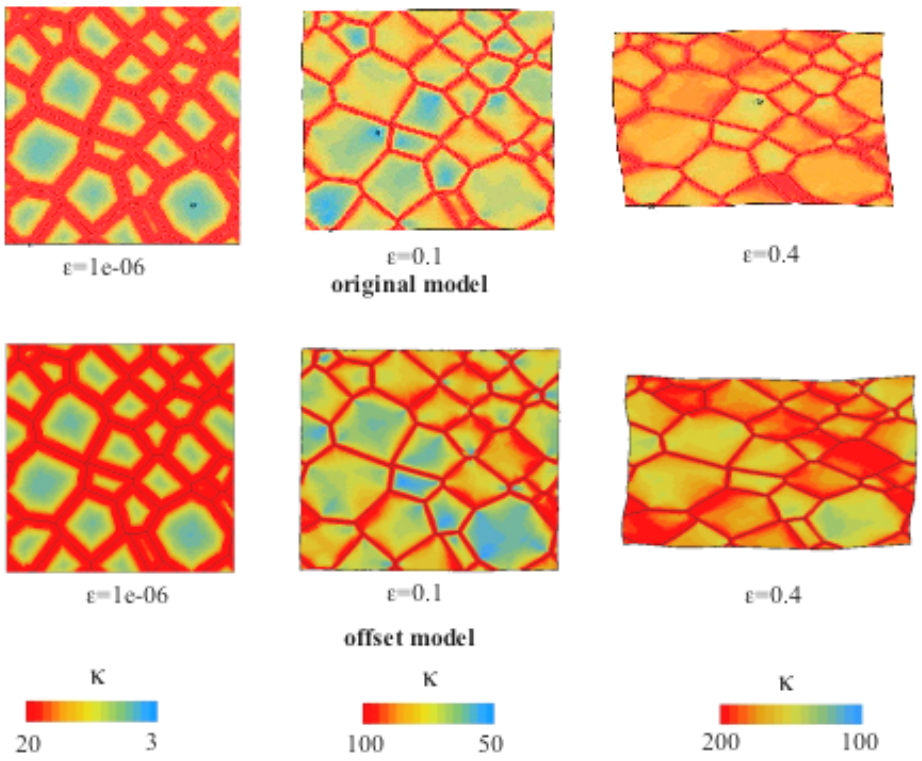

Figure 2. 13 - Comparison of predicted slip system strength distribution using "original" and "offset" grain boundary strengthening models in a polycrystal with an average grain size of 15 μm.

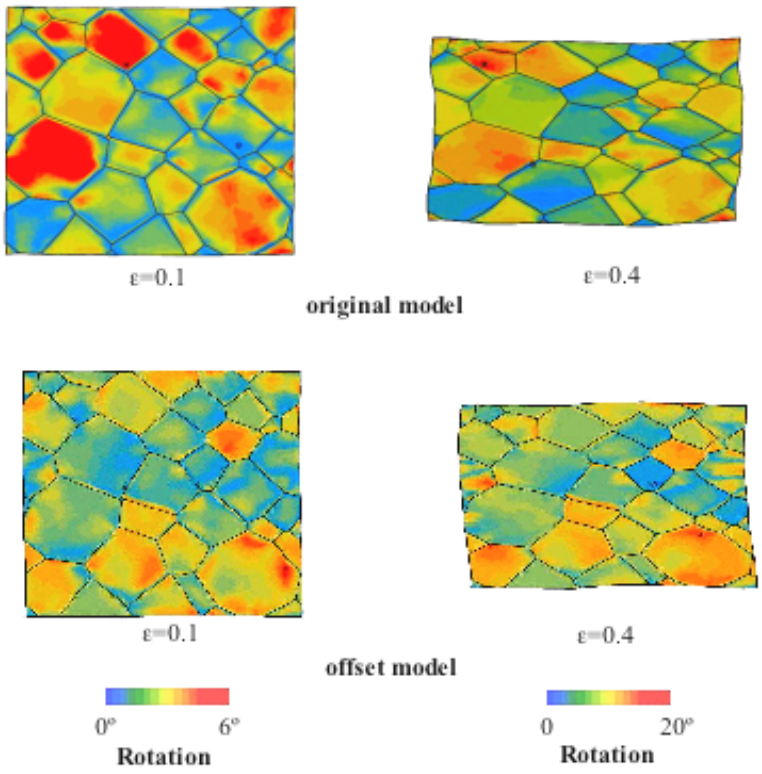

Figure 2. 14 - Comparison of predicted crystallographic misorientation using "original" and "offset" grain boundary strengthening models in a polycrystal with an average grain size of 15 μm.

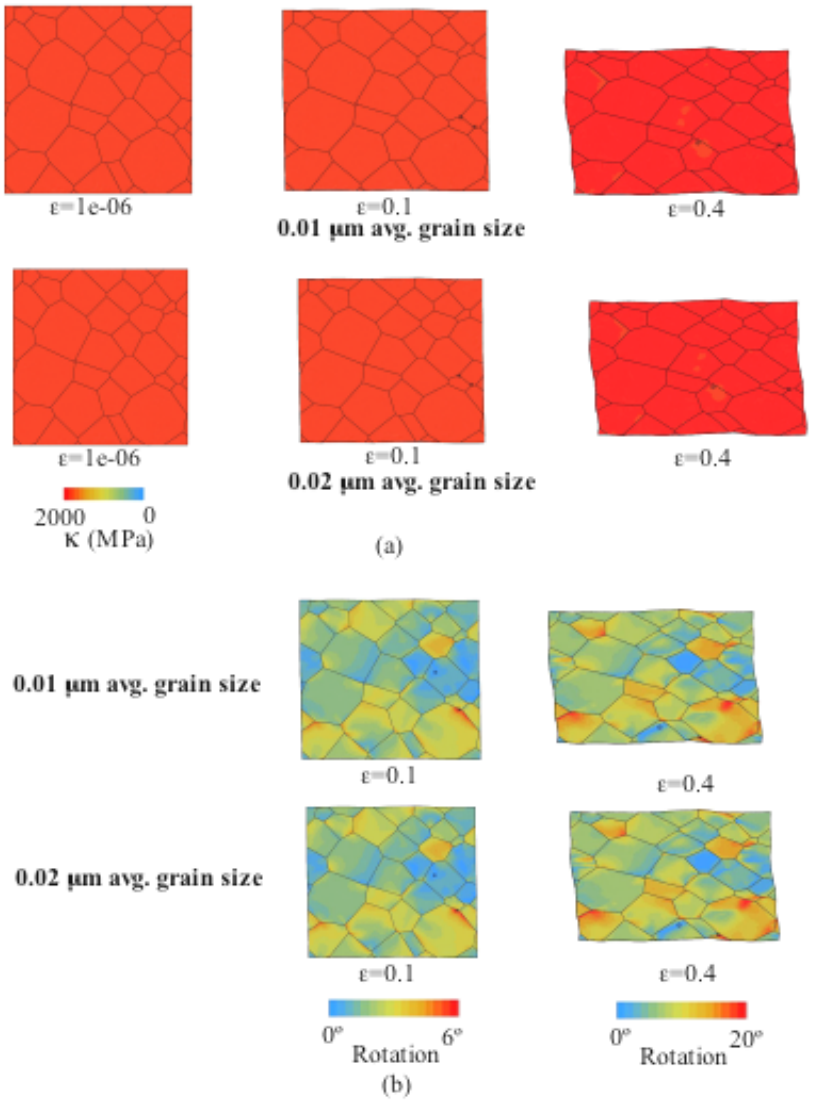

Figure 2. 15- Offset model results of simulated polycyrstals with average grain sizes of 0.01 μm an 0.02 μm. (a) Slip system strength distribution at tensile strains of 1e-06, 0.1 and 0.4 and (b) Spatially resolved crystallographic misorientation relative to original grain orientation at tensile strains 0.1 and 0.4.

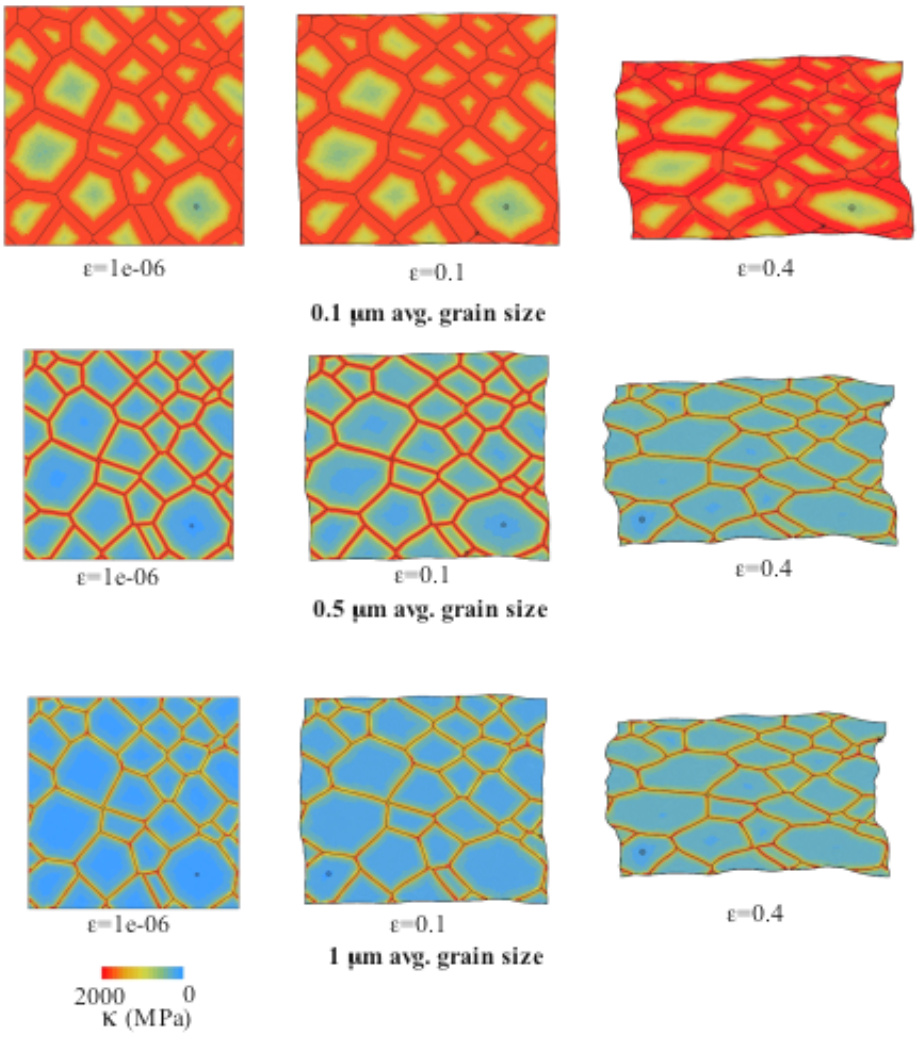

Figure 2. 16 - Predicted slip system strength distribution at tensile strains of 1e-06, 0.1 and 0.4 for polycrystals with average grain sizes of 0.1 μm, 0.5 μm and 1 μm using offset grain boundary strengthening model

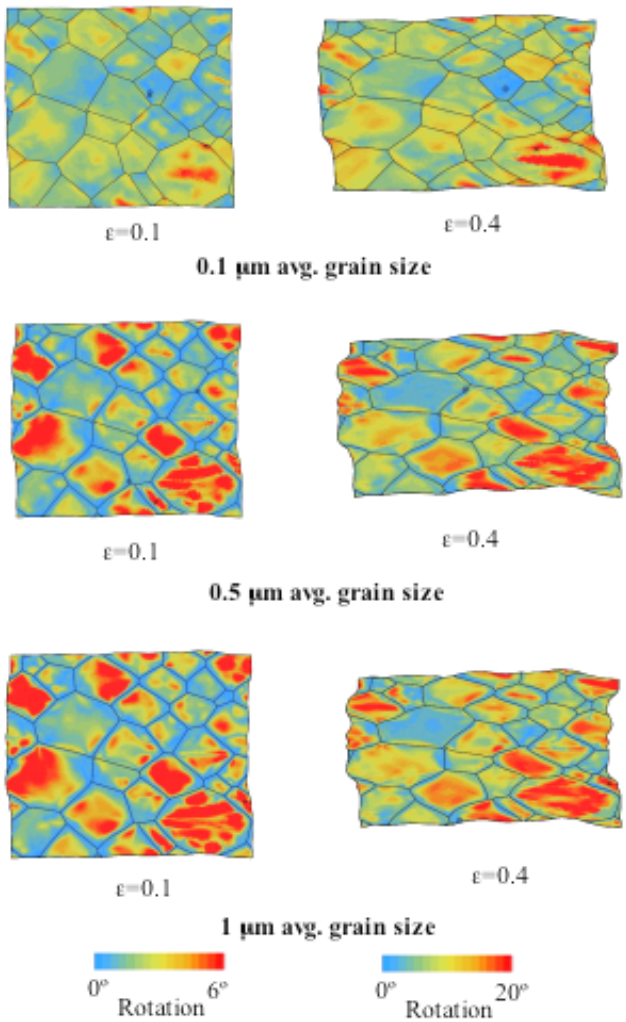

Figure 2. 17 - Predicted spatially resolved crystallographic misorientation relative to original grain orientation at tensile strains 0.1 and 0.4 for polycrystals with average grain sizes of 0.1 μm, 0.5 μm and 1 μm.

3. Modified Strain Gradient Plasticity Model

There are many ways of introducing length scales into plasticity modeling. In recent years considerable effort has been devoted to the development of continuum strain gradient models (e.g. Fleck and Hutchinson [2, 3]), dislocation dynamics and discrete dislocation models (e.g. Needleman [4, 5], Schwarz [6, 7], and Kubin [8, 9]) which are based on direct calculation of interactions of multiple dislocations, and embedded models that incorporate atomistics [10, 11] or discrete dislocation simulations [12, 13] into a higher order computational framework like FEM. Less attention has been paid to the truly non-local models, which allow the state of the continuum in one region of the system depend on that in other regions [14]. The goal of all these models is to predict phenomena that depend on the size of microstructural features, e.g. as described by the Hall-Petch effect wherein the yield strength increases with decreasing grain size as

$$\sigma_y = \sigma_0 + Kd^{-1/2} \tag{3.1}$$

where σ_y denotes the yield stress and d is a grain diameter [1].

Strain gradient methods require additional, higher-order balance equations and cannot be incorporated into the framework of the current code. Dislocation dynamics and discrete dislocation methods, as well as the embedded methods, are either mesoscopic or atomistic and, thus, cannot be directly integrated into a continuum framework. The most promising approach, therefore, is the non-local approach. For the present purpose, we focus on the non-local Taylor-based model introduced by Gao and Huang [15].

The model is based on two fundamental precepts. First is the generalized Taylor relation [16],

$$\tau = \alpha\mu b\sqrt{\rho_S + \rho_G} \tag{3.2}$$

where τ is the flow stress, μ denotes the shear modulus, b is the Burgers vector, $\rho_S$is the density of statistically stored dislocations, ρ_G is the density of geometrically necessary dislocations, and α is an empirical constant typically of order one. Geometrically necessary dislocations are the ones that are needed to accommodate strain incompatibilities and are, as has been long established, related to strain gradients [3]. Statistically stored dislocations are generally thought to be related to plastic strains. Second is the observation that strain gradients can be approximated as integrals of strain fields over infinitesimally small volumes. This development is rather significant because the connection of dislocation densities and strain gradients is well established. With the Gao and Huang approximation, this connection can be generalized to an integral (non-local) formulation.

It is worth noting here that Gao's and Huang's integrals are not truly non-local because they are valid in infinitesimally small volumes only and diverge with increasing volume. This formulation is not ideal for numerical calculations, especially since our goal is to modify an existing code in the specific FEM framework of JAS3D. Therefore, we have modified Gao's and Huang's integrals, writing them as integrals over the whole volume of a deforming body and introducing exponentials that depend on length scale parameters so that these integrals asymptotically converge to Gao and Huang's integrals when the length-scale goes to zero. Thus,

while Gao's and Huang's approximation to the *k* gradient of the *ij* component of a tensor field ε at position x is

$$\varepsilon_{ij,k}(\mathbf{x}) = \frac{\int_{V_{cell}} \left(\varepsilon_{ij}(\mathbf{x}+\boldsymbol{\alpha}) - \varepsilon_{ij}(\mathbf{x})\right) \alpha_m dV}{\int_{V_{cell}} \alpha_m \alpha_k dV} \tag{3.3}$$

ours is

$$\varepsilon_{ij,k}(\mathbf{x}) = \frac{\int_{V_{tot}} \left(\varepsilon_{ij}(\mathbf{x}+\boldsymbol{\alpha}) - \varepsilon_{ij}(\mathbf{x})\right) \alpha_m e^{-C\left(|\alpha_1|+|\alpha_2|+|\alpha_3|\right)} dV}{\int_{V_{tot}} \alpha_m \alpha_k e^{-C\left(|\alpha_1|+|\alpha_2|+|\alpha_3|\right)} dV} \tag{3.4}$$

where V_{cell} is the volume of a region surrounding the position x, V_{tot} is the volume of the entire system, α is a displacement vector from x, and the constant *C* in the exponential serves as a cut-off distance analogous to that for an interatomic potential, but with finite elements instead of atoms. This latter constant eliminates the need to integrate over the entire system volume in practice. Our analyses (for one dimension) established that this approximation is quite good for fields that are changing slower than x^4.

The density of geometrically necessary dislocations can be related to an effective strain gradient η as

$$\rho_G = \frac{2\eta}{b} \tag{3.5}$$

while the density of statistically stored dislocations is determined by the effective plastic strain only. This leads to a law of strain gradient plasticity like

$$\sigma = \sigma_{ref} \sqrt{f^2(\varepsilon) + l\eta} \tag{3.6}$$

where σ_{ref} is a constant, $f(\varepsilon)$ is a function of the form

$$f(\varepsilon) = \frac{3\alpha\mu b\sqrt{\rho_S}}{\sigma_{ref}},$$

and *l* is a length-scale parameter that ensures that the coefficient relating the effective strain gradient η has a dimension of length [16, 15]. Thus, our formulation has two length scales: the cut-off distance *C*, and the length parameter *l*.

This model can be implemented as is, but it is incomplete in one important sense. Consider, for instance, equation (3.5) relating the density of geometrically necessary dislocations to the effective strain gradient. If in the process of deformation the effective strain gradient decreases, the density of geometrically necessary dislocations has to go down according to equation (3.5) because fewer dislocations are needed to accommodate the incompatibility of strain. But dislocations cannot physically disappear just because the applied stress is lifted (and we have not considered processes like recovery here). Physically, it makes more sense to say that geometrically necessary dislocations that are no longer needed to accommodate strain can

become mobile, but they must remain in the system and interact with other dislocations. Some could be annihilated in those interactions, but many will remain and contribute to hardening. In the same manner, the density of statistically stored dislocations cannot be just a function of accumulated plastic strain. After all, even an unstressed material can (and generally does) have statistically stored dislocations in it. This means that we have to consider evolution of different dislocation populations with relation to applied stress to keep track of how many dislocations really are in the system.

The evolution equations for dislocation densities are readily available. These models were developed to study dislocation patterning and plastic instabilities in metals. The best known of these models is due to Walgraef and Aifantis [17, 18, 19] who used reaction and diffusion equations to describe dislocation interactions. A similar model was developed by Ananthakrishna [20].

Walgraef and Aifantis developed [18] spatially dependent dislocation evolution equations of reaction-diffusion type to describe the formation of persistent slip bands (PSB) in metallic materials under cyclic loading. Based on the continuum theory of dislocations, a balance equation like

$$\partial_t \rho + \operatorname{div} j = \hat{c} \tag{3.7}$$

where j is the dislocation flux and $\hat{c}$ represents the production or annihilation of dislocations, forms the basis for the evolution equations. The flux could be determined from a momentum balance or constitutive equation. Considering two different types of dislocations, mobile and immobile, non-linear partial differential equations were derived that described the dominant mechanisms for PSB formation, and these PDE's have the form

$$\partial_t \rho_I = g(\rho_I) - b\rho_I + \rho_M \rho_I^2 + D_I \Delta \rho_I \tag{3.8}$$

and

$$\partial_t \rho_M = b\rho_I - \rho_M \rho_I^2 + D_M \Delta \rho_M \tag{3.9}$$

where the subscripts M and I denote mobile and immobile respectively, ρ is dislocation density, and D is diffusivity.

The generation of immobile dislocations is described by the function $g(\rho_I)$. A corresponding generation term does not appear in the mobile dislocation equation because it is assumed for PSB's that all newly generated dislocations will be immediately pinned. The pinning, or immobilization, of mobile dislocations leads to a decrease in the mobile dislocation density at a rate of $-\rho_M\rho_I^2$ and a corresponding increase in the immobile dislocation density at a rate of $\rho_M\rho_I^2$. Similarly, immobile dislocations break free as a result of stress at a rate $b\rho_I$ causing the population of the immobile dislocations to decrease at a rate $-b\rho_I$ and the population of the mobile dislocations to increase at the same rate. The dislocation motion due to diffusion introduces spatially dependent flux terms, $D_I\Delta\rho_I$ and $D_M\Delta\rho_M$.

Ananthakrishna [20] also developed a set of spatially dependent dislocation evolution equations, taking into account different dislocation types and different dislocation interactions. Rather than considering two dislocation types, he divided the dislocation population into three types: mobile,

immobile, and those with a cloud of solute atoms. Ananthakrishna also based the dislocation evolution equations on the continuity equation but rather than consider flux directly he considered dislocation density and velocity, v, as

$$\partial_t \rho + \partial_i (\rho\, v_i) = \hat{c} \tag{3.10}$$

From this, and a set of dislocation reactions [20], the following set of dislocation evolution equations were derived:

$$\frac{\partial \rho_m}{\partial t} + \frac{\partial}{\partial x_i}(\rho_m v_m) = \theta v_m \rho_m - \mu' \rho_m^2 - \mu \rho_m \rho_{im} + \lambda \rho_{im} - \beta \rho_m \tag{3.11}$$

$$\frac{\partial \rho_{\mathrm{im}}}{\partial \mathrm{t}} + \frac{\partial}{\partial \mathrm{x_i}}(\rho_{\mathrm{im}} \mathrm{v_{im}}) = \mathrm{k}\mu' \rho_{\mathrm{m}}^2 - \mu \rho_{\mathrm{m}} \rho_{\mathrm{im}} - \lambda \rho_{\mathrm{im}} + \beta' \rho_{\mathrm{i}} \tag{3.12}$$

$$\frac{\partial \rho_{\mathrm{i}}}{\partial \mathrm{t}} + \frac{\partial}{\partial \mathrm{x_i}}(\rho_{\mathrm{i}} \mathrm{v_i}) = \beta \rho_{\mathrm{m}} - \beta' \rho_{\mathrm{i}} \tag{3.13}$$

where the subscripts *m*, *im*, and *i* denote mobile, immobile, and solute-clouded dislocations; and θ, μ, λ, β, and k are constants.

Either of these models can be incorporated into our non-local model. Both have length scales, and are therefore able to reproduce dislocation structures. A combined model for dislocation-mediated deformation and dislocation density evolution would possess multiple length scales, making it more realistic. In such a combined approach, geometrically necessary dislocation densities and strain-related statistically stored dislocation densities will determine the production terms of the evolution equations.

Consider, for instance, the Walgraef-Aifantis model. If the effective strain gradient decreases, some of the (previously produced) geometrically necessary dislocations will become mobile. This will modify terms in equation (3.9), since the assumption that all newly produced dislocations are pinned is superfluous in the combined model. An increase in the value of the effective strain gradient, on the other hand, will produce additional geometrically necessary, i.e. immobile, dislocations, determining, together with the plastic strain production, the immobile dislocation production term $g(\rho_i)$ in equation (3.8). The Ananthakrishna model can be combined with the non-local plasticity model in the same manner.

At present, we have implemented into JAS3D the very basics of a non-local model that describes the dependence of ρ_G on the approximated strain gradient, as described above. While the preceding discussion presents in some detail how this basic model for geometrically necessary dislocations could be made more complete and realistic by adding dislocation evolution equations, it is difficult to determine *a priori* which of the two evolution models will be better for our purposes. (Still, the Walgraef-Aifantis model seems preferable because it appears to have fewer assumptions.) Nonetheless, we feel that the incorporation of dislocation density evolution equations into the framework of crystal plasticity will greatly improve the fidelity of the existing models, particularly in predicting microstructure size effects and dislocation patterning.

3.1.References for Section 3

1. Hirth J.P., Lothe J., Theory of Dislocations, Second Edition, Kreieger Publishing Company, Malabar Florida (1982)

2. Fleck N.A., Hutchinson J.W., A reformulation of strain gradient plasticity, Journal of Mechanics and Physics of Solids, 49 (2001) 2245-2271

3. Fleck N.A., Hutchinson J.W, Strain gradient plasticity. In: Hutchinson J.W., Wu T.Y. (Eds) Advances in Applied Mechanics, Vol. 33. Academic Press, New York, NY, pp 295-361

4. Needleman A., Computational mechanics at the mesoscale, Acta Materialia,V. 48(#1) Pp. 105-124 Jan 1, 2000

5. Needleman A., Van Der Giessen E., Discrete dislocation and continuum descriptions of plastic flow, Materials Science And Engineering A-Structural Materials, Properties Microstructure And Processing, V. 309(SISI) Pp. 1-13 Jul 15, 2001

6. Schwarz K.W., Simulation of dislocations on the mesoscopic scale: I: Methods and examples, Journal Of Applied Physics,V. 85(#1) Pp. 108-119 Jan 1, 1999

7. Wickham L.K., Schwarz K.W., Stolken J.S., Rules for forest interactions between dislocations, Physical Review Letters,V. 83(#22) Pp. 4574-4577 Nov 29, 1999Kubin L.P., Estrin Y., Evolution of dislocation densities and the critical conditions for the Portevin-Lechatelier effect, Acta Metallurgica Et Materialia, V. 38(#5) Pp. 697-708 1990

8. Devincre B., Kubin L.P., Mesoscopic simulations of dislocations and plasticity, Materials Science And Engineering A-Structural Materials Properties Microstructure And Processing,V. 234 Pp. 8-14 Aug 30, 1997

9. Devincre B., Kubin L.P., The modelling of dislocation dynamics: elastic behaviour versus core properties, Philosophical Transactions Of The Royal Society Of London Series A-Mathematical Physical And Engineering Sciences,V. 355(#1731) Pp. 2003-2012 Oct 15, 1997

10. Phillips R. Multiscale modeling in the mechanics of materials, Current Opinion in Solid State & Materials Science, v. 3(#6) pp. 526-532 Dec. (1998)

11. Shenoy VB, Miller R, Tadmor EB, Rodney D, Phillips R, Ortiz M, An adaptive finite element approach to atomic-scale mechanics : the quasicontinuum method, Journal of the Mechanics and Physics of Solids, v. 47(#3) pp. 611-642 (1999)

12. Lemarchand C, Chaboche Jl, Devincre B, Kubin L.P., Multiscale modelling of plastic deformation, Journal De Physique Iv,V. 9(#P9) Pp. 271-277 Sep 1999

13. Devincre B., Kubin L.P., Lemarchand C., Madec R., Mesoscopic simulations of plastic deformation, Materials Science And Engineering A-Structural Materials: Properties Microstructure And Processing,V. 309(SISI) Pp. 211-219 Jul 15, 2001

14. Eringen A.C., Continuum Physics, v. 4, Polar and Nonlocal Field Theories, Academic Press, New York and London, 1976

15. Gao H., Huang Y., Taylor-based nonlocal theory of plasticity, International Journal of Solids and Structures, 38 (2001) pp 2615-2637

16. Nix W.D., Gao H., Indentation size effects in crystalline materials: a law for strain gradient plasticity. J. Mech. Phys. Solids 46, pp 411-425

17. Walgraef D, Aifantis E.C., On the formation and stability of dislocation patterns .3. 3-dimensional considerations, International Journal Of Engineering Science, V. 23(#12) Pp. 1365-1372 1985

18. Walgraef D., Aifantis E.C., On the formation and stability of dislocation patterns .1. One-dimensional considerations, International Journal Of Engineering Science, V. 23(#12) Pp. 1351-1358 (1985)

19. Walgraef D., Aifantis E.C., Plastic instabilities, dislocation patterns and non-equilibrium phenomena, Res Mechanica, v. 23(#2-3) pp. 161-195 (1988)

20. Ananthakrishna G. Formation, propagation of bands and chaos in jerky flow, Scripta Metallurgica Et Materialia, v. 29(#9) pp. 1183-1188 (1993)

4. Coupled Simulations of Deformation and Grain Growth

4.1. Interdependence of Mechanics and Microstructure

Thermomechanical processing is very common in a wide variety of manufacturing technologies. In particular, metal forming often involves significant deformation, and this is commonly either performed at elevated temperatures or followed by heat treatment. Deformation can have a substantial effect on material properties, as can microstructural modification of a deformed metal. Therefore, it is important to understand how a material's microstructure, and its evolution, affect mechanical response and *vice versa*.

In this section, front tracking is used to simulate grain growth in an idealized isotropic polycrystal. Deformation is simulated at various stages of grain growth using the finite element method (FEM) with material properties for Cu. The FEM formalism includes anisotropic linear elasticity, crystal plasticity, and isotropic power-law hardening. This coupling between microstructural evolution and deformation, though incomplete, provides valuable insights into the effects of microstructural changes on mechanical response.

4.2. Simulation Methods for Coupling Grain Growth and Deformation

4.2.1. Front tracking model for grain growth

Grain growth is energetically advantageous because it reduces the total grain boundary area. The velocity, v, of a moving grain boundary is proportional to the pressure, P, driving its motion [1], such that

$$v = MP \tag{4.1}$$

where M is the boundary's mobility. The driving pressure always acts normal to the boundary. In a pure, defect-free polycrystal, boundary motion is driven by the curvature of the grain boundaries, and the driving pressure is $P_\kappa = \gamma\kappa$, where γ is the grain boundary energy per unit area (or length in two dimensions) and κ is its curvature. The curvature pressure acts toward the center of curvature.

In a stressed, elastically anisotropic material where the elastic energy changes across a grain boundary, the total elastic energy in the material will change (even without stress redistribution) as the grain boundary moves. Therefore, stored elastic energy can drive boundary migration in a stressed, elastically anisotropic material, and the driving pressure is simply the difference in stored elastic energy density across the boundary, $P_e = \Delta H_e$, where [2]

$$H_e = \frac{1}{2}\boldsymbol{\sigma}\boldsymbol{\varepsilon}_e \tag{4.2}$$

and $\boldsymbol{\sigma}$ and $\boldsymbol{\varepsilon}_e$ are the stress and elastic strain tensors, respectively.

In a plastically deformed material, the motion of a grain boundary can remove dislocations from its wake. Assuming that all defects are removed from the material when a boundary passes

through it, the plastic driving pressure is simply the stored plastic energy density ahead of the moving boundary, $P_p = H_p$, where [2]

$$H_p = \frac{(\tau_o - \tau_i)^2}{2\alpha^2 G} \tag{4.3}$$

α is a constant, and G is the shear modulus equal to C_{44} (see Table I).

The elastic and plastic pressures act toward the grain with higher stored energy. Thus, in an elastic-plastically deformed material with curved grain boundaries, assuming all driving pressures operate with a common mobility, the grain boundary velocity is

$$v = M(P_k + P_e + P_p) \tag{4.4}$$

Although the present grain growth simulations do not include the effects of deformation, incorporating these effects is a goal of this work, and the elastic and plastic driving forces will be examined here using the deformation results.

To apply this model to a practical simulation of grain growth [1], a topologically realistic, two-dimensional grain structure is created in the computer by representing the grain boundaries as curved line segments that terminate at the triple junctions. In practice, this grain structure is mapped from a Monte Carlo Potts [3] result. The boundary line segments are discretized by uniformly distributing points along them. The curvatures at each point are calculated by fitting a circle to the point of interest and its two nearest neighbor points on the same boundary, and taking the curvature to be the inverse of the circle's radius, $\kappa = 1/r$. The velocity of each point can then be calculated using equation (4.1), with the driving pressure set to P_κ. A time step, Δt, is chosen such that $\Delta t = \Delta x_{max}/v_{max}$, where Δx_{max} is a predetermined maximum allowable point displacement. Each point is moved by a distance $\Delta x = v\Delta t$ toward the center of the fitted circle (see above), and the entire procedure is repeated.

4.2.2. Polycrystal plasticity model for deformation

The front tracking simulations provide grain microstructures at various stages of evolution. The grain boundaries are represented by points that connect the triple junctions. To model the deformation of these microstructures, the grain boundary points are used as a nodal framework to create a finite element mesh. The regions between the boundary points, i.e. the grain interiors, are paved with quadrilateral elements using Sandia's FASTQ mesh generation code. The resulting two-dimensional mesh is duplicated and offset to produce a three-dimensional mesh of hexahedra that is one element thick. Each grain is assigned an individual crystallographic orientation from a random distribution.

The deformation model follows the standard kinematic framework [4, 5] from an anisotropic elastic and isotropic plastic material. In addition, the slip rate, $\dot{\gamma}$, on each slip system is defined as [6]

$$\dot{\gamma} = \dot{\gamma}_o \frac{\tau}{\tau_o} \left| \frac{\tau}{\tau_o} \right|^{\frac{1}{m}-1} \tag{4.5}$$

where $\dot{\gamma}_o$ is a reference slip rate, τ is the resolved shear stress on the slip system, τ_o is the critical resolved shear stress, and m is the rate sensitivity factor. The critical resolved shear stress evolves according to the isotropic hardening law

$$\tau_o = \tau_i + A\varepsilon_p^n \tag{4.6}$$

where τ_i is the initial (unhardened) value and ε_p is the equivalent plastic strain. A and n are constants. The values of all elastic and plastic material constants used in the deformation model are provided in Table I.

The deformation of the polycrystal is simulated using Sandia's JAS3D code, which is a quasi-static nonlinear conjugate gradient finite element solver. Periodic boundary conditions are imposed in all directions, and the mesh is deformed by 1% in the y-direction ("up/down" in the figures shown here) and held there.

Table I. Material constants for Cu. *C*ij are elastic constants, and the remaining symbols are defined in the text.

Constant	Value
C_{11}	168.4 GPa
C_{12}	121.4 GPa
C_{44}	75.4 GPa
$\dot{\gamma}_o$	1.0
τ_o	6.21 MPa
m	0.05
A	283.51 MPa
n	0.729
α	0.5

4.3.Results of Coupled Simulations

Figure 4.1 shows the distributions of elastic and plastic strain energy density in the polycrystal, as defined by equations (4.2) and (4.3), respectively, at various stages of grain growth and after 1% elongation. The dimensions of the simulation cells are 200 x 200 in arbitrary units. The finite element meshes have a thickness of 1. The stored elastic energy density is almost an order of magnitude larger than the plastic energy density. However, because the elastic driving force for grain growth depends on the difference in stored energy density across a grain boundary, and the plastic driving force is the larger of the two energy densities at the boundary, the elastic and plastic driving forces for grain growth are actually comparable in this case.

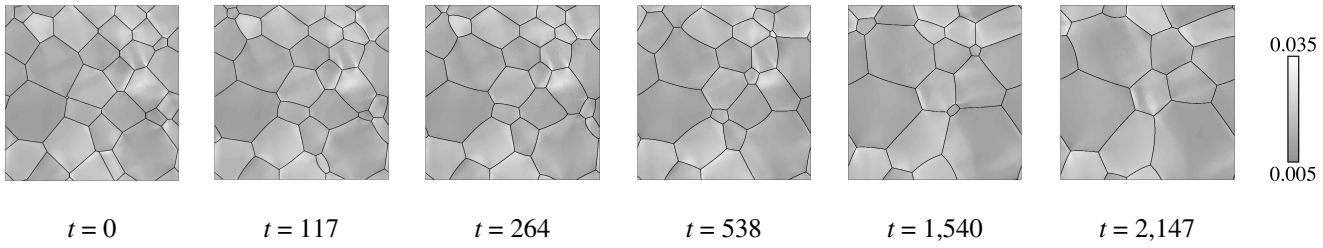

(a)

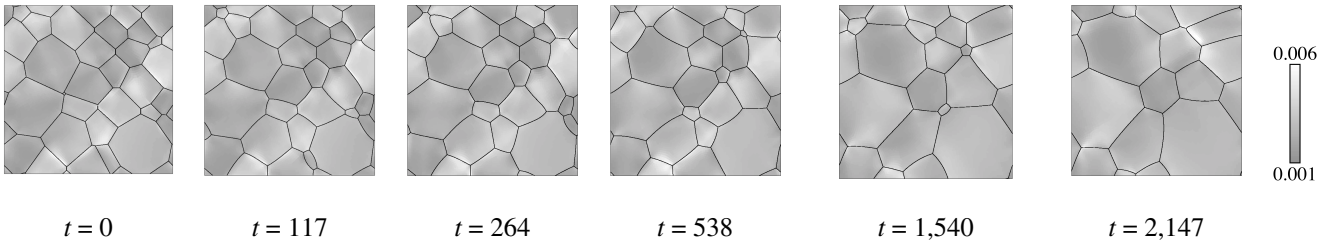

(b)

Figure 4.1. Distributions of a) elastic and b) plastic strain energy density at various stages of grain growth. Energy densities are in units of MPa.

While the local details of the strain energy distributions change as the grain topology changes, the qualitative features of these distributions remain largely unchanged. Grains with low average strain energy density (dark gray) generally stay that way, and the same is true for high-energy regions (light gray). This suggests that the details of the grain topology do not substantially affect overall mechanical response. Figure 4.2 shows the elastic and plastic strain energy densities in the polycrystal deformed 1% after $t = 538$ of grain growth, but with a set of random grain orientations different than that in figure 4.1. Clearly, the stored energy distributions in figures 4.2a and 2b are very different from those in the corresponding (fourth) frames in figures 4.1a and 1b, indicating that the overall strain energy density distributions are controlled primarily by the orientations of the individual grains.

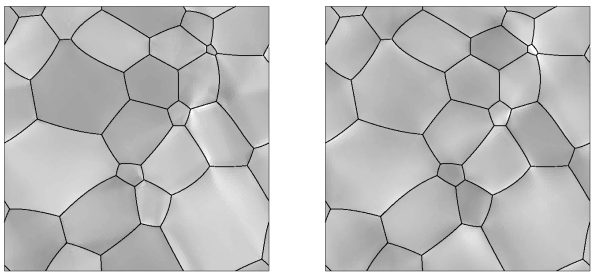

(a) (b)

Figure 4.2. Distributions of a) elastic and b) plastic strain energy density after $t = 538$ of grain growth, with a different set of random grain orientations than in figure 4.1.

At 1% elongation, elastic strain energy density is almost an order of magnitude larger than plastic strain energy density. Nonetheless, the elastic and plastic driving forces for grain growth

are comparable. Overall elastic and plastic strain energy distributions depend primarily on the orientations of individual grains, rather than grain boundary network topology.

4.4.References for Section 4

1. H.J. Frost, C.V. Thompson, C.L. Howe, and J. Whang, *Scr. Metall.* **22** (1988) 65.

2. G.E. Dieter, *Mechanical Metallurgy*, 3rd Ed. (McGraw-Hill 1986).

3. D.J. Srolovitz, M.P. Anderson, P. Sahni, and G. Grest, *JOM* **35** (1982) A83.

4. R. Hill and J.R. Rice, *J. Mech. Phys. Solids* **20** (1972) 401.

5. R.J. Asaro and J.R. Rice, *J. Mech. Phys. Solids* **25** (1977) 309.

6. J.W. Hutchinson, *Proc. Roy. Soc. Lond. A* **348** (1976) 101.

5. Appendix A: Publications and Presentations

5.1. Publications

C. C. Battaile, E. A. Holm, T. Buchheit, G. Wellman, and M. Neilsen, "Coupled Simulations of Mechanical Deformation and Microstructural Evolution Using Polycrystal Plasticity and Monte Carlo Potts Models," *Mat. Res. Soc. Symp. Proc.* **538** 269-273 (1999).

C. C. Battaile, T. Buchheit, G. W. Wellman, M. K. Neilsen and E. A. Holm, "Coupled Simulations of Deformation and Grain Growth," *Fourth Pacific Rim International Conference on Advanced Materials and Processing (PRICM4)*, S. Hanada, Z. Zhong, S. W. Nam and R. N. Wright (editors) (Japan Institute of Metals, Tokyo, 2001) pp. 763-765.

E. A. Holm and C. C. Battaile, "Computer Simulations of Microstructural Evolution," *JOM* **53**[9] 20-23 (2001) and in *JOM-e* at http://www.tms.org/pubs/journals/JOM/0109/Holm-0109.html.

T.E. Buchheit, G.W. Wellman, and B.L. Boyce, "The Role of Microstructure in MEMS Deformation and Failure," *Proceedings from Deformation and Damage Characterization of Micro/Nano Materials* (2002).

T. E. Buchheit, G. W. Wellman, and C. C. Battaile, "Exploring the Limits of Polycrystal Plasticity Modeling," submitted to *Mechanics of Materials* (2002).

5.2. Invited Presentations

C. C. Battaile, T. E. Buchheit, E. A. Holm, G. W. Wellman, and M. K. Neilsen, "Simulating Microstructural Evolution in Deformed Polycrystals," (Invited) TMS Fall Meeting, Cincinnati, OH, November 1999.

E. A. Holm, "Advances in modeling grain growth and recrystallization," (Invited) ASM Materials Solutions 2001, Indianapolis, IN, November 2001.

T. E. Buchheit, G. W. Wellman, M. K. Neilsen, C. C. Battaile, and E. A. Holm, "Exploring the Limits of Finite Element Based Polycrystal Plasticity Modeling," (Invited) Mechanics Department Seminar, Brown University, Providence, RI, January 2002.

E. A. Holm, C. C. Battaile, and W. A. Counts, "Stress Effects on Microstructural Evolution in Textured Polycrystals," (Invited) MRS Spring Meeting 2002, San Francisco, CA, April 2002.

C. C. Battaile, "Coupled Simulations of Deformation and Grain Growth," (Invited) Third Workshop on Microstructural Effects on the Mechanics of Materials, Los Alamos, NM, May 2002.

C. C. Battaile, "Coupled Simulations of Deformation and Grain Growth," (Invited) Gordon Conference on Physical Metallurgy, Plymouth, NH, July 2002.

T.E. Buchheit, J.R. Michael, G.W. Wellman, and C.C. Battaile, "Characterizing the Role of Microstructure on the Properties of Microsystems Materials," (Invited) Princeton University Seminar Series, Princeton, NJ, 2002.

5.3. Contributed Presentations

T.E. Buchheit, D.A. LaVan, G.W. Wellman and M.K. Neilsen, "Comparison Between Simulation and Experiment of a Polycrystal Plasticity Deformation Model", TMS Fall Meeting, Cincinnati Ohio, November 1999.

T.E. Buchheit, G. Wellman, "Predicted Evolution of a Flow Surface by a Polycrystal Deformation Model", MRS Fall Meeting Symposium C, Boston, Massachusetts, November 1999.

T. E. Buchheit, C. C. Battaile, G. W. Wellman, E. A. Holm, "Providing a Length Scale by Capturing the Influence of Grain Boundaries in Polycrystal Plasticity Modeling," TMS Annual Meeting 2002, Seattle, WA, February 2002.

C. C. Battaile, "Coupled Simulations of Deformation and Grain Growth," Fifth Workshop on Anisotropic Interface Properties, Gaithersburg, MD, March 2002.

C. C. Battaile, "Coupled Simulations of Deformation and Grain Growth," Sandia Complex Materials Forum, Albuquerque, NM, June 2002.

T.E. Buchheit, G.W. Wellman, and B.L. Boyce, "The Role of Microstructure in MEMS Deformation and Failure," 2002 ASME International Mechanical Engineering Congress, New Orleans, LA, November 2002.

Distribution:

10	MS1411	Elizabeth A. Holm, 1834
5	1411	Corbett C. Battaile, 1834
5	1411	H. Eliot Fang, 1834
1	0893	Rebecca Brannon, 09123
5	0893	Gerald W. Wellman, 09123
5	0889	Thomas E. Buchheit, 1851
1	0889	Richard J. Salzbrenner, 1851
2	0899	Technical Library, 9616
1	0612	Review and Approval Desk, 9612 For DOE/OSTI
1	0188	LDRD Office, 1010
1	9018	Central Technical Files, 8945-1